THE FLOW OF PURE VAPOR UNDERGOING FILM CONDENSATION BETWEEN PARALLEL PLATES

By

A. NARAIN

and

Y. KIZILYALLI

IMA Preprint Series # 502

February 1989

THE FLOW OF PURE VAPOR UNDERGOING FILM CONDENSATION BETWEEN PARALLEL PLATES

A. Narain and Y. Kizilyalli

Department of Aerospace Engineering and Mechanics*
University of Minnesota
Minneapolis, MN 55455

Abstract: The flow of pure saturated vapor between parallel plates, with film condensation on the bottom plate, is considered and a *genuine* approximate solution is obtained. The mixed differential-integral approach of this paper predicts film-thickness profile, condensation rate, wall heat transfer rate, and other quantities of interest. Most importantly, the non-linearities of the flow predict a new phenomenon of formation of recirculating zones beyond a certain distance downstream of the flow.

* Regular address (after August 1989):
Department of Mechanical Engineering and Engineering Mechanics
Michigan Technological University
Houghton, MI 49931

1. Introduction

Flows involving pure vapor with film condensation on walls have received extensive attention in engineering literature. These flows are important in the design of direct contact heat exchangers [1] as well as in some novel compact heat removal systems for space applications ([2], [3]). Despite this, some of the more fundamental studies of these flows have been limited to condensing external flows over flat plates (Nusselt [4], Rohsenow [5], Sparrow and Gregg [6], etc.) or over drops (Ford and Lekic [7], Jacobs and Cook [8], Sundarajan and Ayyaswamy [9], etc.). Most of the existing studies involving flow in ducts, both experimental and theoretical ([10], [11], [12], [13], [14]), provide only partial, but useful, results on certain aspects of such flows. Therefore there is a need for fundamental studies of these flows which will shed light on the evolving complexity of vapor velocity profiles, the location of the interface, as well as the usual physical quantities (wall heat transfer rates, condensation rate, etc.) of engineering interest. However, fundamental predictions and analysis have proved to be difficult because even the simplest realistic mathematical models for such flows are written in terms of highly non-linear partial differential equations with an unknown boundary.

With the above as a motivation, we choose to study the flow of pure saturated vapor entering the confined region between two horizontal parallel plates (see Fig. 1.1). As in many realistic situations, we assume that the pressure gradient along the vapor flow is small and therefore pressure everywhere is approximately the inlet pressure p_∞. This means that the flow is driven primarily by the momentum flux at the inlet (prescribed inlet velocity profile). For a simplified analysis, we assume that the vapor and the upper plate is at a saturation temperature of T_s (p_∞) and the lower plate is at a constant wall temperature of $T_w < T_s$ (p_∞). This usually leads to film condensation on the bottom plate. The reader should note that if the incoming vapor was allowed to have a small superheat, this would only affect the results of this paper in a small quantitative manner, and not in any significant qualitative manner (see a similar result in Fig. 4.3 of [15] for flow over a flat plate). We begin our analysis by employing a complete and nearly exact theory (Delhaye [16], [17]) for dynamic condensation of pure vapors. This is particularly important because there has been some confusion ([18], see p. 486) with regard to interface conditions on phase change boundaries. For

applications, however, we simplify the governing equations and the interface conditions to a realistic differential model for the problem at hand (see Fig. 1.1). The simplified equations, on integration, lead to the usual control-volume equations [19] found in engineering literature (see section 2 for a brief review).

We solve the governing non-linear free boundary problem by projecting all the essential features of the governing equations into a system of non-linear ordinary differential equations. However, the method introduced in this paper differs from the usual integral solution approaches ([14], [19]) in two significant ways: (i) the integral approximation is used only for one of the variables (the vapor velocity profile) of the problem and the remaining differential restrictions of the model are satisfied exactly; and (ii) an error measure is defined and computed which indicates the difference between the computed solution and the solution of the differential model. In this way, we are able to choose our approximation for vapor velocity in such a way that the error is small at all points of interest in the flow field and therefore we have a genuine approximate solution. Therefore, when experimental predictions are not easily available, the method of this paper and the usual finite difference (see, e.g., [20]) or finite element schemes could be used and a good comparison between the discrete and the integral approaches would lead to reliable flow predictions. While the underlying philosophy of our solution approach is classical ([21], [22]), its actual implementation for this problem would not have been possible without the use of modern computer capabilities for symbolic manipulations and high-precision numerical solution of a system of non-linear ordinary differential equations.

The computed solution for the problem at hand is in qualitative agreement with the wall-heat transfer and film thickness profile observations in a related experiment [23]. In the experiments of Christodoulou and Suryanarayana [23], as in our theory, the condensation of R-113 vapor leads to an approximately constant film thickness profile. These observations [23] are not compatible with the flat plate theory ([24], [25], [6], [15]) but they are in qualitative agreement with our predictions. In the reported experiments [23], the vapor flow prior to the inlet is such that they have, in all likelihood (see section 9), a fully *turbulent* vapor flow at the inlet. Since our theory is for *laminar* flows, we currently have no experiments available with which we can quantitatively compare the predictions reported here. We note, however, that for many turbulent vapor flows at the inlet, condensation causes a rapid loss in vapor momentum and the flow should

laminarize beyond a certain downstream distance L_{tr}. Therefore the method of this paper applies to all situations in which the transitional distance L_{tr} is either zero or sufficiently small compared to the length of interest in the downstream direction.

One of the most interesting flow phenomena predicted by our computations is the *understandable* appearance of recirculating zones, beyond a certain distance downstream, in the core of the vapor flow. This phenomenon is qualitatively illustrated in Fig. 1.1 below and the existence of these zones is inferred from the velocity profiles obtained in section 8. However, an experimental confirmation of the existence of such recirculating zones is currently not available.

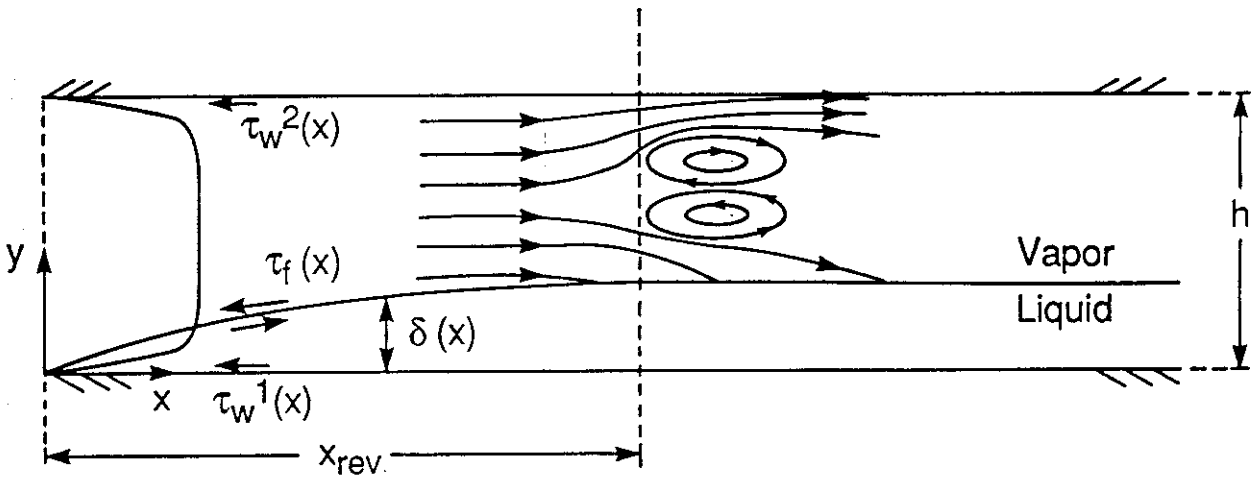

Figure 1.1: In the flow above, a laminar flow of pure vapor enters the parallel plate configuration at $x = 0$. The flow is steady with vapor occupying $\delta(x) \leq y \leq h$ and liquid occupying $0 \leq y \leq \delta(x)$ at any given x. The stream line patterns and a reversal distance x_{rev} are inferred from computational results presented in section 8. The shear stresses $\tau_w^1(x)$, $\tau_f(x)$ and $\tau_w^2(x)$ respectively act at the bottom plate ($y = 0$), the interface ($y = \delta(x)$), and the upper plate ($y = h$).

2. Simplified Control Volume Equations

In this section, we briefly recall the well-known [19] simplified control volume equations for the flow depicted in Figure 1.1. The exact theory and approximations leading to the derivation of the simplified control volume equations is presented later in sections 3 and 4.

The flow in the narrow gap of Fig. 1.1 is believed to be adequately modeled under the following assumptions:

(i) Pure vapor enters the parallel plate configuration at $x = 0$ (see Fig. 1.1) at a pressure of p_∞ and at a temperature equal to the corresponding saturation temperature of $T_s(p_\infty) \equiv T_s$.

(ii) There is no significant pressure drop along the direction of flow. This means that the flow is primarily driven by the inertia of the incoming vapor.

(iii) The flow is steady and the film thickness $\delta(x)$ varies only moderately with x.

(iv) For x within certain bounds, the velocity and temperature variations perpendicular to the direction of flow outweigh the velocity and temperature variations in the direction of flow.

(v) The bottom plate is kept at a constant temperature $T_w < T_s(p_\infty)$ while the top plate is maintained at the temperature of the incoming saturated vapor $T_s(p_\infty)$.

(vi) $(T_s - T_w)/T_s$ is small enough that the fluid properties (density ρ_I, conductivity k_I, specific heat $(C_p)_I$, viscosity μ_I, etc.) can be treated essentially as constants in each phase ($I = 1$ for liquid, $I = 2$ for vapor). Therefore each property (e.g., density) undergoes a sudden jump during condensation across the interface.

Let $u_1(x, y)$ be the x-component of the velocity field in the liquid phase, $T_1(x, y)$ be the temperature field in the liquid phase, $u_2(x, y)$ be the x-component of the velocity field in the vapor phase, and $T_2(x, y) = T_s(p_\infty)$ be the constant temperature field in the vapor phase. Furthermore let $\delta(x)$, $\dot{m}(x)$, and $u_f(x)$ respectively denote the film thickness of the liquid condensate, mass condensation rate across the interface, and the approximate common value of the tangential components of the liquid and vapor

velocities at the interface (i.e., $u_f(x) \equiv u_1(x, \delta(x)) = u_2(x, \delta(x))$). The simplified control volume equations [19] for the flow in Fig. 1.1 are summarized below.

Mass balance for the vapor: This states that

$$\frac{d}{dx} \int_{\delta(x)}^{h} \rho_2 u_2 (x, y)\, dy \equiv -\dot{m}(x)\,, \tag{2.1}$$

where $\dot{m}(x) > 0$ indicates mass transfer from the vapor to the liquid across the interface.

Momentum balance for the vapor: This simplifies to

$$\frac{d}{dx} \int_{\delta(x)}^{h} \rho_2 u_2^2 (x, y)\, dy + \dot{m}(x)\, u_f(x) = -\frac{\partial \bar{p}_2}{\partial x} - \tau_w^2(x) - \tau_f(x)\,, \tag{2.2}$$

where for *laminar* flows $\tau_w^2(x) \equiv -\mu_2 \frac{\partial u_2}{\partial y}(x, h)$, $\tau_f(x) \equiv \mu_2 \frac{\partial u_2}{\partial y}(x, \delta(x))$, and the mean pressure gradient $\partial \bar{p}_2/\partial x$ is assumed to be approximately zero for the flow in Fig. 1.1.

Energy balance for the vapor phase: The control volume equations for the vapor flow in Fig. 1.1, under usual approximations [19], is given as

$$\frac{d}{dx} \int_{\delta(x)}^{h} \rho_2 c_{p_2} T_2 u_2\, dy + \dot{m} h_g = -q_w(x) + q_f(x)\,, \tag{2.3}$$

where for *laminar* flows $q_f(x) \equiv -k_2 \frac{\partial T_2}{\partial y}(x, \delta)$ and $q_w(x) \equiv -k_2 \frac{\partial T_2}{\partial y}(x, h)$. This equation, with $h_g = C_{p_2} T_s$, is trivially satisfied for the constant temperature field $T_2(x, y) = T_s$.

Mass balance for the liquid phase: This simplifies to

$$\frac{d}{dx} \int_{0}^{\delta(x)} \rho_1 u_1\, dy = \dot{m}(x)\,, \tag{2.4}$$

where $\dot{m}(x)$ is same as in (2.1).

Momentum balance for the liquid phase: This simplifies to

$$\frac{d}{dx}\int_0^{\delta(x)} \rho_1 u_1^2 (x, y)\, dy - \dot{m}(x)\, u_f(x) = -\frac{\partial \bar{p}_1}{\partial x} - \tau_w^1 (x) + \tau_f(x) , \tag{2.5}$$

where $\tau_w^1(x) \cong \mu_1 \frac{\partial u_1}{\partial y} (x, 0)$, $\tau_f(x) \cong \mu_1 \frac{\partial u_1}{\partial y} (x, \delta(x))$. We see later in section 4 that under assumptions of small liquid inertia and negligible mean pressure gradient $\frac{\partial \bar{p}_1}{\partial x}$, equation (2.5) further simplifies to

$$\tau_w^1(x) \cong \tau_f(x) . \tag{2.6}$$

Energy balance for the liquid phase: This condition, under usual simplifications [19], is given by

$$\frac{d}{dx}\int_0^{\delta(x)} \rho_1 C_{p_1} u_1 T_1\, dy - \dot{m} h_f = q_w(x) - q_f(x) , \tag{2.7}$$

where $q_w(x) \cong -k_1 \frac{\partial T_1}{\partial y} (x, 0)$ and $q_f(x) \cong -k_1 \frac{\partial T_1}{\partial y} (x, \delta(x))$. Under the assumption of negligible convection of energy downstream, it can be seen (see section 4) that (2.7) reduces to pure conduction across the film as given by

$$q_w(x) - q_f(x) \cong 0 . \tag{2.8}$$

We now present the interface condition relevant to our modeling of the flow in figure 1.1.

Continuity of tangential component of velocities: This condition, as shown later in sections 3 and 4, reduces to

$$u_1 (x, \delta(x)) = u_2 (x, \delta(x)) = u_f (x) . \tag{2.9}$$

Continuity of shear along the interface: This condition for laminar flows, again as shown in sections 3 and 4, simplifies to

$$\mu_1 \frac{\partial u_1}{\partial y}(x, \delta(x)) = \mu_2 \frac{\partial u_2}{\partial y}(x, \delta(x)) \tag{2.10}$$

Normal stress condition at the interface: We show later in sections 3, 4, and 9 that for a suitable lower bound on the values of x (say $x > \bar{\varepsilon}$), this condition simplifies to

$$p_1(x, \delta(x)) = p_2(x, \delta(x)) . \tag{2.11}$$

Energy transfer condition at the interface: This condition reduces to

$$\dot{m}(x) h_{fg} = k_1 \frac{\partial T_1}{\partial y}(x, \delta(x)) - k_2 \frac{\partial T_2}{\partial y}(x, \delta(x)) , \tag{2.12}$$

where $h_{fg} \equiv h_g - h_f$ is the jump in the value of enthalpy (latent heat) across the interface. Note that h_g and h_f are, respectively, values of enthalpy for saturated vapor and saturated liquid at the saturation temperature T_s (p_∞). These are easily determined from standard thermodynamic tables [26].

3. Exact Governing Equations and Interface Conditions for Film Condensation Over Surfaces

In this chapter, we review and study the fundamental equations governing dynamic film condensation of pure vapors (see Delhaye [16] or Narain and Lee [15]). We present these exact equations for the sake of a complete specification of various physical phenomena and to assess the validity of the simplified equations in sections 2, 4, and 5 as a model for the flow in Fig. 1.1.

It is assumed that the fluid in its vapor or liquid phase is adequately characterized as a compressible Newton-Fourier substance with regard to its constitutive relations for stress and heat flux. The thermodynamic characterizations are, as is commonly accepted, the measurements on the same substance under approximate *homogeneous* (all flow variables are spatially uniform) or equilibrium processes (e.g.,

see sections 1.5 and 1.6 of Batchelor [27]). These characterizations are available in classical thermodynamics tables and texts ([26], [28]).

We choose to denote the liquid phase by subscript $I = 1$ and the vapor phase by subscript $I = 2$. Let, in either phase at any point $\mathbf{x}$ at time t, $\mathbf{T}_I$ be the Cauchy Stress, $\mathbf{v}_I$ be the velocity field, μ_I be the viscosity, κ_I be the usually small and ignorable *expansion viscosity* (see Batchelor, [27], p. 154 or White, [29], p. 70 for a discussion), p_I be the thermodynamic pressure field, ρ_I be the density field, k_I be the thermal conductivity, $\hat{u}_I$ be the internal energy per unit mass, T_I be the temperature field, ∇T_I be the temperature gradient field, $\mathbf{D}_I$ be the field associated with the symmetric part of the velocity gradient $\nabla \mathbf{v}_I$. Then, for $I = 1$ or 2, the stress constitutive relations are

$$\mathbf{T}_I = -p_I \mathbf{1} + \mathbf{S}_I \text{ , where } \mathbf{S}_I \equiv 2\mu_I \mathbf{D}_I + \kappa_I (\text{div } \mathbf{v}_I)\, \mathbf{1}, \tag{3.1}$$

and the heat flux ($\mathbf{q}_I$) relations are

$$\mathbf{q}_I = -k_I \nabla T_I \,. \tag{3.2}$$

The Continuity, Momentum, and Energy equations in either of the phases are

$$\frac{\partial \rho_I}{\partial t} + \nabla \cdot (\rho \mathbf{v}_I) = 0 \,,$$

$$\rho_I \frac{d\mathbf{v}_I}{dt} = \rho_I \mathbf{g} + \text{div } \mathbf{T}_I \,,$$

and

$$\rho_I \frac{d\hat{u}_I}{dt} = -\nabla \cdot \mathbf{q}_I + \text{tr } (\mathbf{T}_I \mathbf{D}_I) \,. \tag{3.3}$$

The momentum equation $(3.3)_2$ for the liquid phase ($I = 1$) is often modified (see [30]) to account for solid-fluid interactional forces if the film condensate is very thin (10-1000 Å, 1 Å = 10^{-10} m). However, the theory in this paper is for those flows for which the condensate thickness is large enough (greater than 1/100 mm) to disregard these forces and the associated phenomenon of rupture [30]. Since the equations of state for these classical fluids are modeled to be the same as in a homogeneous process, we may use the relations (see [28]) of the type

$$\hat{u}_I = \hat{u}_I(\rho_I, T_I), \quad p_I = p_I(\rho_I, T_I). \tag{3.4}$$

Though the viscosities μ_I, κ_I, and conductivities k_I do not appear in any homogeneous process, the following characterization for them is known to be adequate ([29], p. 77)

$$\mu_I = \mu_I(\rho_I, T_I), \kappa_I = \kappa_I(\rho_I, T_I), \text{ and } k_I = k_I(\rho_I, T_I). \tag{3.5}$$

In any specific condensation problem, equations (3.1)–(3.5) have to be solved subject to appropriate initial and boundary conditions (at wall, at infinity, or at inlet/outlet boundaries of the flow domain) relevant to the problem. In addition, one has to impose the interface conditions which account for the physical processes at the liquid-vapor interface.

The conditions to be imposed at an interface experiencing film condensation or film boiling had been a source of confusion (see Whitaker [18], p. 486) until Delhaye ([16], [17]) derived them from first principles. The derivation involves considering an arbitrary material-volume around the interface such that the interface lies *within* this volume with the liquid on one side and the vapor on the other. One then applies the mass, momentum, and energy balance principles to the material volume while accounting for the fact that there is a moving interface within this element. The limiting form of these equations as the material volume collapses to the interface provides the resulting interface conditions. The results of this analysis ([16], [17]) are listed below.

Kinematic conditions at the interface: Let $I(\mathbf{x}, t) = 0$ be the equation of the interface at any time t. If one considers the interface positions at times t and $t + \Delta t$ and then considers *any* one to one mapping of the two positions, one can define (locally in time) an interfacial motion $\mathbf{x}(t)$ of every point on the interface. However, for any such choice of a one to one map described above, the surface velocity $\mathbf{v}_S(\mathbf{x}, t) \equiv \frac{d\mathbf{x}(t)}{dt}$ is easily seen to satisfy (see [33])

$$\mathbf{v}_S \cdot \mathbf{n} \equiv -\frac{\frac{\partial I}{\partial t}}{\nabla I}, \tag{3.6}$$

where $\mathbf{n}(\mathbf{x}, t)$ is taken to be a unit normal on the interface directed from the liquid to the vapor phase.

Continuity of tangential velocities: Since the fluids are Newtonian, it is reasonable to assume continuity of the tangential components of interfacial velocities $\mathbf{v}_1^i$ and $\mathbf{v}_2^i$. This is written as

$$\mathbf{v}_1^i \cdot \mathbf{t} = \mathbf{v}_2^i \cdot \mathbf{t} \equiv \mathbf{v}_s \cdot \mathbf{t} \equiv v_t \,, \tag{3.7}$$

where $\mathbf{t}$ is any unit tangent vector on the interface. The equations (3.6) and (3.7) together completely define the surface speed $\mathbf{v}_s$.

Mass balance at the interface: This condition reduces to

$$\rho_1 \{(\mathbf{v}_1^i - \mathbf{v}_s) \cdot \mathbf{n}\} = \rho_2 \{(\mathbf{v}_2^i - \mathbf{v}_s) \cdot \mathbf{n}\} \equiv - \dot{m} (\mathbf{x}, t) \,, \tag{3.8}$$

where the unit normal $\mathbf{n}$ is directed from the liquid phase to the vapor phase.

Momentum balance at the interface: This condition reduces to

$$\left[\dot{m} (\mathbf{x}, t) \mathbf{v}_1^i - \dot{m} (\mathbf{x}, t) \mathbf{v}_2^i\right] + \left[(p_2^i - p_1^i) \mathbf{n}\right]$$
$$+ \left[(\mathbf{S}_2^i - \mathbf{S}_1^i) \mathbf{n}\right] + \left[-\{\nabla_s \sigma - (\nabla_s \cdot \mathbf{n}) \sigma \mathbf{n}\}\right] = 0 \tag{3.9}$$

The first, second, third and fourth terms in (3.9) respectively account for the net momentum flux per unit area, pressure difference, viscous stress difference ($\mathbf{S}_I$ is defined in (3.1)), and surface tension. Since surface tension coefficient σ is defined only on the interface, the surface terms $\nabla_s(\cdot)$ have usual differential geometric meanings (see formulas on p. 53 and p. 223 of Weatherburn [31]). From here and henceforth, the superscript "i" on the right side of any variable (as in terms of (3.7)–(3.9)) denotes the interfacial value of the flow variable in the appropriate fluid phase.

Energy balance at the interface: If one defines enthalpy per unit mass as

$$h_I \equiv u_I + \frac{p_I}{\rho_I}, \text{ and surface velocity as } \mathbf{v}_s \equiv (\mathbf{v}_s \cdot \mathbf{n})\,\mathbf{n} + (v_{to}\mathbf{t}_o)\ , \qquad (3.10)$$

then the energy balance reduczes to

$$\left[\dot{m}\,(h_1^i - h_2^i)\right] + \left[\frac{1}{2}\,\dot{m}\,\left|\mathbf{v}_1^i - \mathbf{v}_s\right|^2 - \frac{1}{2}\,\dot{m}\,\left|\mathbf{v}_2^i - \mathbf{v}_s\right|^2\right]$$
$$+ \left[\left(\mathbf{S}_1^i\mathbf{n}\right)\cdot\left(\mathbf{v}_1^i - \mathbf{v}_s\right) - \left(\mathbf{S}_2^i\mathbf{n}\right)\cdot\left(\mathbf{v}_2^i - \mathbf{v}_s\right)\right]$$
$$+ \left[-k_2\,\frac{\partial T_2}{\partial n}\,\Big|^i + k_1\,\frac{\partial T_1}{\partial n}\Big|^i\right]$$

$$+ \left[-\nabla_s \cdot (\sigma v_{to}\mathbf{t}_o) + \{\nabla_s\sigma - (\nabla_s \cdot \mathbf{n})\,\sigma\,\mathbf{n}\}\cdot\mathbf{v}_s\right] = 0\ . \qquad (3.11)$$

In (3.11), the first term accounts for 'latent heat', the second term accounts for changes in kinetic energy across a moving interface, the third term accounts for differences in viscous working at the interface ($\mathbf{S}_I$ was defined in (3.1)), the fourth term accounts for the net interfacial heat transfer through conduction, and the fifth term accounts for working due to surface tension.

Interface equations of state: The conditions (3.6)–(3.11) are quite general and could be used for any material undergoing a phase change across an interface. However, to be able to use these conditions, we now specify the fluid and the associated values of interfacial enthalpies (h_I^i , I = 1 or 2). It is recalled that for these fluids undergoing a homogeneous process, the saturation temperature $T_s = T_s(p)$ is determined by the pressure p alone (see [28], p. 35). Therefore, it is assumed that the same holds locally in a non-homogeneous process and the temperatures T_I^i (I = 1 or 2) on the two sides of the interface must satisfy

$$T_I^i = T_s\,(p_I^i)\ , \qquad (3.12)$$

where p_I^i are values of interfacial pressures on the corresponding sides of the interface at any given point **x** and time t. Furthermore, since the enthalpy h_I in (3.10) can be characterized (see p. 77 of [29]) as $h_I = h_I\,(p_I\ ,\ T_I)$, the enthalpy at the interface h_I^i in (3.11) is to be found through

$$h_I^i = h_I\,(p_I^i\,,\ T_s\,(p_I^i)) \qquad (3.13)$$

for I = 1 or 2.

The conditions (3.6)–(3.13) constitute a complete specification of the interface conditions.

4. Approximations and Scaling of the Governing Flow Equations

In this section, we outline the scaling arguments to decide which terms of the governing equations and interface conditions are significant and which are not. It is assumed that the liquid condensate is thin ($\delta(x)/x \ll 1$) for most values of x of interest in the flow of Fig. 1.1. Although this flow is very different from the flow over a flat plate (Sparrow and Gregg [6], Koh [24], Narain and Lee [15], etc.), we find that the scaling arguments ([32], [15]) for this flow are similar and they lead to boundary layer *type* equations whenever h/x is small (narrow gap, see Fig. 1.1). The only physical consequence of this assumption $\left(\frac{\partial^2 u_2}{\partial x^2} \ll \frac{\partial^2 u_2}{\partial y^2}\right)$ is that one ignores the contribution of $\mu_2 \frac{\partial v_2}{\partial x}$ in the expression of $\tau_f(x)$ given in (2.2). This means that the assumption should be good for large x/h (say $x/h \geq 2$) and *perhaps* adequate for $0 \leq x/h \leq 2$ (there being no physical reason for substantial inaccuracies).

We now list the approximations to the exact equations in two categories: (a) constancy of various flow parameters, and (b) the scaling analysis which identifies the significant physical phenomena and retains only the corresponding significant terms.

(a) Constancy of Flow Parameters

(i) It is assumed that "$(T_s\,(p_\infty) - T_w) / T_\infty$", and "$(p - p_\infty) / p_\infty$" are small and lead to a low Mach number for the vapor flow. This means that we can consider the density of the vapor to be

$$\rho_2 = \rho_2\,(p_2,\ T_2) \cong \rho_2\,(p_\infty,\ T_s)\ , \qquad (4.1)$$

where $T_s \cong T_s(p_\infty)$. Under approximations similar to the one leading to (4.1), for I = 1 or 2, we write

$$\rho_I \cong \rho_I(p_\infty, T_s),\ \mu_I \cong \mu_I(\rho_I, T_s), \text{ and } k_I \cong k_I(\rho_I, T_s). \tag{4.2}$$

We note that the right sides of (4.2) are constants for both I = 1 and I = 2.

(ii) As a consequence of the incompressibility approximation $(4.2)_1$, the pressures p_I (I = 1 or 2) away from the interface, are no longer treated as thermodynamic variables as they become constitutively indeterminate reaction pressure fields (see Truesdell [33]). The pressure fields are now determined only by the equations governing the flow dynamics and the prescription of the pressure on the flow boundaries.

(iii) The implications of constant densities ρ_I on the enthalpy equation of state $h_I = h_I(p_I, T_I)$ is that the effects of a jump in density across the phase change boundary (e.g. see Fig. 3.3., p. 35 of [28]) need only be considered by accounting for the jump in enthalpy (h_{fg}) across the interface. We see later in (4.23) that there is a very slight jump in pressure across the interface and this is the reason why pure vapor sharply turns into pure liquid (without going through a mixture zone) across the interface. The assumption of approximately constant densities and pressure fields for the liquid and vapor phases allows us to write (see (1.5.19), p. 27 of Batchelor [27])

$$(C_p)_I \cong (C_p)_I \Big|_{\rho = \rho_I \text{ and } T_I = T_s}, \tag{4.3}$$

as approximate constants for I = 1 and 2.

We are now in a position to use the approximations (4.2)–(4.3) and write the equations governing the flow in Figure 1.1. As we are interested in steady flow in the x-y plane, we consider the velocity fields

$$\mathbf{v}_I(\mathbf{x}) = u_I(x, y)\,\mathbf{i} + v_I(x, y)\,\mathbf{j} \tag{4.4}$$

and the temperature fields T_I (x, y) for each phase (I = 1 or 2). The no-slip conditions for this flow are

$$u_1 (x, 0) = v_1 (x, 0) = 0 ,$$

and

$$u_2 (x, h) = v_2 (x, h) = 0 . \tag{4.5}$$

The wall temperature condition and the saturated vapor conditions are

$$T_1 (x, 0) = T_w ,$$

and

$$T_2(x, y) = T_s \tag{4.6}$$

for $x \geq 0$ and $\delta(x) \leq y \leq h$.

(b) Scaling Leading to Steady Boundary Layer Type Equations

We now list the scaling assumptions and approximations in the spirit of Kocamustafaoğullari [32] and Narain and Lee [15].

(i) For most values of x (of representative length L) away from zero, in a narrow gap between the plates, we have

$$\varepsilon_1 \equiv \frac{\delta(L)}{L} \ll 1 \quad \text{and} \quad \varepsilon_2 \equiv \frac{h}{L} \ll 1 . \tag{4.7}$$

(ii) It is expected, since there is no significant pressure gradient, that in both the liquid and vapor flows, viscous forces are comparable to inertia forces. This is written as

$$O\left(\mu_I \nabla^2 \mathbf{v}_I\right) \sim O\left(\rho_I \frac{d\mathbf{v}_I}{dt}\right) \tag{4.8}$$

for each phase (I =1 or 2). From here and henceforth we use the symbol O (z (x, y)) to represent the mean size of a variable z over the domain variables x and y.

(iii) Let the order of magnitude of the x-component of the liquid's interfacial speed $u_f(x) \equiv u_1 (x, \delta(x))$ be

$$O\,(u_1\,(x,\,\delta(x)) \sim u_1\,(L,\,\delta(L) \equiv U_1\ , \tag{4.9}$$

and the order of magnitude of the average vapor speed at a typical x(~L) be U_2. We now introduce scaled variables with a superscript '+' in such a way that the approximate size of any scaled variable is O(1). These variables are defined as

$$x \equiv Lx^+,\ \frac{y-0}{\delta(L)} \equiv y_1^+ \text{ for } 0 \le y \le \delta(x)\,,$$

$$\frac{u_1\,(x,y)}{U_1} \equiv u_1^+\,(x^+,\,y^+)\,,\ \frac{u_2\,(x,\,y)}{U_2} \equiv u_2^+\,(x^+,\,y^+)\ ,$$

$$\frac{T_s-T_1\,(x,\,y)}{(T_s-T_w)} \equiv T_1^+\,(x^+,\,y^+)\,,\ \ T_2^+\,(x^+,\,y^+) \equiv \frac{T_2\,(x,\,y)}{T_s} = 1. \tag{4.10}$$

(iv) From here and henceforth, the mean size of a derivative $\frac{\partial z}{\partial \xi}$ for $\alpha_1 < \xi < \beta_1$ and and $\hat{\alpha}_1 < \eta < \hat{\beta}_1$ is denoted by $O\left(\frac{\partial z}{\partial \xi}\ (\xi\ ,\ \eta)\right)$ and it is to be interpreted as a quantity equal to

$$\left.\frac{\Delta z}{\Delta \xi}\right|_{\eta=\eta_m} = \frac{\{z(\beta_1,\,\eta_m)-z(\alpha_1,\,\eta_m)\} \div N}{\{\beta_1-\alpha_1\} \div N}$$

$$= \frac{z(\beta_1,\,\eta_m)-z(\alpha_1,\,\eta_m)}{\beta_1-\alpha_1}, \tag{4.11}$$

where $\eta_m = O(\eta)$ is the mean representative value of the variable η and N is any large positive number. With the help of $(3.3)_1$, $(4.2)_1$, (4.4), (4.10), and (4.11), one concludes that

$$O(v_I) \sim \varepsilon_I U_I \tag{4.12}$$

for I=1 and 2

Therefore we set

$$v_I \equiv \varepsilon_I U_I v_I^+ \tag{4.13}$$

for I=1 and I=2.

(v) Though the pressure in each phase is expected to be close to the inlet pressure p_∞, we still introduce a non-dimensional pressure field p_I^+ (I = 1 or 2) as

$$p_I^+ \equiv \frac{p_I - p_\infty}{\rho_I U_I^2} \quad . \tag{4.14}$$

With the help of all the definitions and scalings introduced thus far, it is easy to verify that (4.8) yields

$$Re_1\varepsilon_1^2 \sim O(1) \, , \; Re_2\varepsilon_2^2 \sim O(1) \, , \tag{4.15}$$

where $Re_I \equiv \frac{\rho_I U_I L}{\mu_I}$ for I = 1 or 2.

We now use the results in (4.1)–(4.15) to scale the governing equations and the interface conditions. The continuity equation $(3.3)_1$,under (4.10) and (4.13), scales to

$$\frac{\partial u_I^+}{\partial x^+} + \frac{\partial v_I^+}{\partial y_I^+} = 0 \tag{4.16}$$

for I = 1 or 2 and no summation on I. The x-component of momentum equation $(3.3)_2$, for I = 1 or 2, scales to

$$u_I^+ \frac{\partial u_I^+}{\partial x^+} + v_I^+ \frac{\partial u_I^+}{\partial y_I^+} = -\frac{\partial p_I^+}{\partial x^+} + \frac{1}{Re_I\varepsilon_I^2} \frac{\partial^2 u_I^+}{\partial y_I^{+2}} + O(\varepsilon_I^2) \, . \tag{4.17}$$

The momentum equation $(3.3)_2$ in the y-direction scales to

$$\frac{\partial p_I^+}{\partial y_I^+} = -\varepsilon_I (gL/U_I^2) + O(\varepsilon_I^2) \quad . \tag{4.18}$$

We now define a small positive number ε_* as

$$\varepsilon_*^2 \equiv \max\left(\varepsilon_1^2 , \varepsilon_2^2 , \varepsilon_1 \varepsilon_2\right) . \tag{4.19}$$

The energy equation $(3.3)_3$, for I = 1 or 2, under the verifiable assumptions $O\left(Ec_1 \equiv U_1^2 / C_{p_1} (T_s - T_w)\right) = O(\varepsilon_*^2)$ and $0\left(Ec_2 \equiv U_2^2 / C_{p_2} T_s\right) = O(\varepsilon_*^2)$ reduces to

$$u_I^+ \frac{\partial T_I^+}{\partial x^+} + v_I^+ \frac{\partial T_I^+}{\partial y_I^+} = -\frac{1}{Pr_I Re_I \varepsilon_I^2} \frac{\partial^2 T_I^+}{\partial y_I^{+2}} + O(\varepsilon_I^2) . \tag{4.20}$$

We note that for I = 2, (4.20) is trivially satisfied as $T_2^+ (x^+, y^+) = 1$.

The interface condition (3.7) given in (A1.2) of Appendix A1 reduces to

$$u_1^+ \Big|^i = u_2^+ \Big|^i + 0(\varepsilon_*^2) . \tag{4.21}$$

The mass transfer condition (3.8) given in (A1.3) simplifies a little and it is written as

$$\dot{m} \equiv \rho_1 U_1 \varepsilon_1 \dot{m}_1^+ \equiv \rho_2 U_2 \varepsilon_2 \dot{m}_2^+ , \tag{4.22}$$

where

$$\dot{m}_1^+ \equiv \left\{ u_1^+ \frac{d\delta^+}{dx^+} - v_1^+ \right\} .$$

Under the reasonable and subsequently verifiable assumption $O(\sigma/\rho_1 U_1^2 L) = O(\varepsilon_1)$, we find that (A1.5) reduces to

$$\dot{m}_1^{+2} \varepsilon_1^2 \left(\frac{\rho_1}{\rho_2} - 1 \right) + \left\{ \frac{\rho_2}{\rho_1} p_2^+ \Big|^i - p_1^+ \Big|^i \right\} + O(\varepsilon_*^2) = 0. \tag{4.23}$$

In (4.23), the first term corresponds to pressure increase across the interface due to the penetration of vapor momentum through the interface. We show later in section 9 that

this effect is negligible for $x > \bar{\varepsilon}$, where $\bar{\varepsilon}$ is typically quite small. For this reason, we further approximate (4.23) as

$$\left\{ \frac{\rho_2}{\rho_1} p_2^+ \Big|^i - p_1^+ \Big|^i \right\} \cong 0. \tag{4.24}$$

Next we find that the interface momentum balance (3.9) in the tangential direction given by (A1.6) reduces to

$$\left. \frac{\partial u_1^+}{\partial y_1^+} \right|^i - \frac{\mu_2}{\mu_1} \frac{\varepsilon_1}{\varepsilon_2} \left. \frac{\partial u_2^+}{\partial y_2^+} \right|^i + O(\varepsilon_*^2) = 0 \ . \tag{4.25}$$

Furthermore, for the problem in Figure 1.1, there is no imposed pressure gradient and we see, through (4.18) and (4.24), that the pressure is nearly continuous across the interface. The scaled form of (3.18) as given by (A1.8) can now be approximated as

$$T_1^+ (x^+, \delta^+ (x^+)) = T_s^+ (p_1^+ \mid^i) \cong T_s^+ (p_\infty^+) \equiv T_s^+ \ , \tag{4.26}$$

and

$$T_2^+ (x^+, \delta^+ (x^+)) = T_s^+ (p_2^+ \mid^i) \cong T_s^+ (p_\infty^+) \equiv T_s^+ \ .$$

The values of interfacial enthalpies, in physical variables, are

$$h_1^i = h_1 (p_1^i \ , T_s (p_1^i)) \cong h_1 (p_\infty \ , T_s (p_\infty)) \equiv h_f \ ,$$

and

$$h_2^i = h_2 (p_2^i \ , T_s (p_2^i)) \cong h_2 (p_\infty \ , T_s (p_\infty)) \equiv h_g \ . \tag{4.27}$$

Using the notation $h_{fg} \equiv h_g - h_f$, $Ja \equiv h_{fg} / C_{p1} (T_s - T_w)$ and making the verifiable assumption $O(\sigma U_1 / k_1 [T_w - T_s]) = O(\varepsilon_1)$, the interfacial energy transfer condition (3.11) as given by (A1.7) reduces to

$$-JaPr_1(Re_1\varepsilon_1^2) \dot{m}_1^+ - \frac{\varepsilon_1}{\varepsilon_2} \frac{k_2}{k_1} \left. \frac{\partial T_2^+}{\partial y_2^+} \right|^i + \left. \frac{\partial T_1^+}{\partial y_1^+} \right|^i + O(\varepsilon_*^2) = 0 \ . \tag{4.28}$$

For convenience, we now rewrite the scaled equations (4.16), (4.17), (4.18), (4.20)–(4.22), (4.24)–(4.28) in terms of the original physical variables using the definitions in (4.10), (4.13) and (4.14). The resulting equations, along with (4.5) and (4.6), are listed below for either phase (I = 1 or 2).

$$\frac{\partial u_I}{\partial x} + \frac{\partial v_I}{\partial y} = 0, \quad \rho_I\left[u_I \frac{\partial u_I}{\partial x} + v_I \frac{\partial u_I}{\partial y}\right] = -\frac{\partial p_I}{\partial x} + \mu_I \frac{\partial^2 u_I}{\partial y^2},$$

$$\frac{\partial p_I}{\partial y} = -\rho_I g, \quad u_I \frac{\partial T_I}{\partial x} + v_I \frac{\partial T_I}{\partial y} = \alpha_I \frac{\partial^2 T_I}{\partial y^2}, \tag{4.29}$$

where $\alpha_1 \equiv k_1 / \rho_I (C_p)_I$ and $\partial p_I / \partial x \cong 0$.

The interface conditions at $y = \delta(x)$ are

$$p_1 (x, \delta(x)) = p_2 (x, \delta(x)), \; \mu_1 \frac{\partial u_1}{\partial y} (x, \delta(x)) = \mu_2 \frac{\partial u_2}{\partial y} (x, \delta(x)),$$

$$u_1 (x, \delta(x)) = u_2 (x, \delta(x))$$

$$\dot{m}(x)\, h_{fg} = k_1 \frac{\partial T_1}{\partial y}(x, \delta(x)) - k_2 \frac{\partial T_2}{\partial y}(x, \delta(x)),$$

$$T_1 (x, \delta(x)) = T_2 (x, \delta(x)) = T_s ; \tag{4.30}$$

the wall conditions at $y = 0$ are

$$u_1 (x, 0) = v_1 (x, 0) = 0 \text{ and } T_1 (x, 0) = T_w ; \tag{4.31}$$

and the conditions at $y = h$ are

$$u_2 (x, h) = v_2 (x, h) = 0 ,$$
$$T_2 (x, h) = T_s . \tag{4.32}$$

The mass transfer rate $\dot{m}(x)$ in $(4.30)_4$ is given, with the help of (4.22), as

$$\dot{m}(x) = \rho_1\left[u_1 (x, \delta(x)) \frac{d\delta}{dx} - v_1 (x, \delta(x))\right]$$
$$= \rho_2\left[u_2 (x, \delta(x)) \frac{d\delta}{dx} - v_2 (x, \delta(x))\right] . \tag{4.33}$$

While seeking a solution of (4.29)–(4.33), one has to note the simplifications resulting from

$$T_2 (x, y) = T_s \tag{4.34}$$

for $x \geq 0$ and $\delta(x) \leq y \leq h$. Furthermore, (4.29)–(4.34) is to be solved subject to a prescribed inlet velocity profile

$$u_2(0, y) = \tilde{u}(y) \tag{4.35}$$

such that

$$\tilde{u}(0) = \tilde{u}(h) = 0 . \tag{4.36}$$

Assuming no condensation for $x < 0$, compatibility with (4.36) requires the additional initial conditions of

$$\delta(0) = 0$$

and

$$u_1(x, \delta(x)) \Big|_{x=0} = u_2(x, \delta(x)) \Big|_{x=0} = 0 . \tag{4.37}$$

However, the scaling leading to the equations (4.29)–(4.34) are not expected to be valid for $0 \leq x \leq \bar{\varepsilon}$, for some small $\bar{\varepsilon} > 0$, because:

(i) $1/\delta(x)$ is not defined at $x = 0$ as $\delta(0) = 0$; and

(ii) The approximation (4.24) of (4.23), and (4.7) is not valid near $x = 0$.

An a-priori estimate of the errors introduced in modeling the flow in Fig 1.1 by the equations (4.29)–(4.37) is difficult. However, if the leading edge zone $0 \leq x \leq \bar{\varepsilon}$ is small, then we expect that the errors will be small.

We now discuss two substantial simplifications of the model equations governing the flow of the liquid condensate. Our experience with the problem of a uniform flow of pure vapor over a flat plate ([6], [15], [24]) (with *typical* flows of R12 (Freon), R-113, steam, etc.) suggests that as vapor condenses into liquid, there is a huge increase in density with very little forces to drive the liquid condensate (except for the requirement of continuity of velocities and shear stresses at the interface), the resulting flow of the liquid condensate is very sluggish. This means both inertia and convective heat transfer in the direction of the flow are effectively zero. This fact is evident in Figures

4.1–4.2 of Narain and Lee [15] where the liquid temperature and velocity profiles are found to be linear despite the fact that full non-linearities of inertia and convective heat transfer were retained in the model equations as well as in the solution scheme. Further recall that for both the flat plate problem ([25], [15]) and the parallel plates problem of Fig. 1.1, the ratio of viscous forces to inertia in the liquid condensate are comparable and are given by (see 4.17)

$$Re_1 \varepsilon_1^2 \sim 1 \ , \tag{4.38}$$

and the ratio of net conductive and convective heat transfers for liquid flow are comparable and given by (see 4.20)

$$\frac{1}{Pr_1 \ Re_1 \ \varepsilon_1^2} \sim \frac{1}{Pr_1} \ . \tag{4.39}$$

The numerical results of Fig. 4.1 and 4.2 in Narain and Lee [15] establish, despite the fact that the size ratios in (4.38) and (4.39) are still true, that each side of the equations $(4.29)_2$ and $(4.29)_4$ for I = 1 are separately close to zero. Therefore $(4.29)_2$ for the liquid simplifies to

$$\frac{\partial^2 u_1}{\partial y^2} \equiv 0 \ , \tag{4.40}$$

for $x > 0$ and $0 \le y \le \delta(x)$, and $(4.29)_4$ for the liquid simplifies to

$$\frac{\partial^2 T_1}{\partial y^2} \equiv 0 \tag{4.41}$$

for $x > 0$ and $0 \le y \le \delta(x)$. Now (4.40) and (4.41) explain the linearity of velocity and temperature profiles for the liquid as found by Koh [24] and Narain and Lee [15]. Since, on the average at all values of x, we expect smaller inertia of the incoming vapor in the flow between parallel plates (Fig. 2.1) than in the flow over a flat plate ([24], [15]), it is again reasonable to assume that (4.40) and (4.41) suffice as replacements of $(4.29)_2$, and $(4.29)_4$ for I = 1 in the system of equations (4.29)–(4.37). We now introduce a notation $u_f(x)$ in $(4.30)_3$ as

$$u_1(x, \delta(x)) = u_2(x, \delta(x)) \equiv u_f(x) . \tag{4.42}$$

Solving (4.40) subject to $(4.31)_1$ and (4.42), it is easily seen that

$$u_1(x, y) = \frac{u_f(x)}{\delta(x)} y \tag{4.43}$$

for $x > 0$ and $0 \le y \le \delta(x)$. Similarly solving (4.41) subject to $(4.30)_5$ and $(4.31)_2$, it is easily seen that

$$T_1(x, y) = T_w + (T_s - T_w)\, y / \delta(x) . \tag{4.44}$$

In addition to the expressions (4.43) and (4.44), the relevant remaining equations for $u_2(x, y)$,$v_2(x, y)$ and $v_1(x, y)$ in (4.29)–(4.37) are

$$\frac{\partial u_I}{\partial x} + \frac{\partial v_I}{\partial y} = 0 \qquad (I = 1 \text{ or } 2) ,$$

$$\rho_2 \left[u_2 \frac{\partial u_2}{\partial x} + v_2 \frac{\partial u_2}{\partial y} \right] = \mu_2 \frac{\partial^2 u_2}{\partial y^2} ,$$

$$\frac{\partial u_2}{\partial y}(x, \delta(x)) = \frac{\mu_1}{\mu_2} \frac{u_f(x)}{\delta x} ,$$

$$u_2(x, \delta(x)) = u_f(x) ,$$

$$\dot{m}(x)\, h_{fg} = k_1 \frac{T_s - T_w}{\delta(x)} , \tag{4.45}_{1\text{-}12}$$

$$\dot{m}(x) = \rho_1 \left[u_f(x) \frac{d\delta}{dx} - v_1(x, \delta(x)) \right]$$

$$= \rho_2 \left[u_f(x) \frac{d\delta}{dx} - v_2(x, \delta(x)) \right],$$

$$T_2(x, y) = T_s \qquad \text{for} \qquad x > 0 \text{ and } \delta(x) \le y \le h \ ,$$

$$u_2(x, h) = 0 \ ,$$

$$v_2(x, h) = 0 \ ,$$

$$u_2(0, y) = \tilde{u}(y) \quad \text{where} \quad \tilde{u}(0) = \tilde{u}(h) = 0 \ ,$$

$$\delta(0) = 0 \ ,$$

$$u_f(0) \equiv u_2(0, 0) = 0 \ .$$

5. Relation Between the Simplified Differential Equations and the Control Volume Equations

Our strategy is now to solve equations (4.45) by an approximate integral method which satisfies all the equations in (4.45) exactly except for the equation $(4.45)_2$ which we only wish to satisfy approximately. For this purpose, we now integrate some of the equations in (4.45) and relate them to the control-volume equations in section 2. Using $(4.45)_1$, (4.42), $(4.31)_1$, and $(4.32)_1$, it is easy to see that $(4.45)_6$ can be rewritten as

$$\dot{m}(x) = \frac{d}{dx} \int_0^{\delta(x)} \rho_1 u_1 (x, y) \, dy = -\frac{d}{dx} \int_{\delta(x)}^{h} \rho_2 u_2 (x, y) \, dy \ . \tag{5.1}$$

Observe that (5.1) is the same as (2.1) and (2.4) in section 2. Using $(4.45)_1$ for I = 2, $(4.45)_6$, and $(4.45)_9$, and integrating $(4.45)_2$ over y from $y = \delta(x)$ to $y = h$, we find

$$\frac{d}{dx} \int_{\delta(x)}^{h} \rho_2 u_2^2 (x, y) \, dy + \dot{m}(x) u_f(x) = \mu_2 \frac{\partial u_2}{\partial y} (x, h) - \mu_2 \frac{\partial u_2}{\partial y} (x, \delta(x)) \ . \tag{5.2}$$

Note that (5.2) is the same as (2.2) in section 2. We now replace $(4.45)_1$, $(4.45)_2$, and $(4.45)_6$ by (5.1) and (5.2) and retain the remaining restrictions of (4.45). Note that (4.43)–(4.45) are such that the remaining control-volume equations and interface conditions of section 2 are satisfied.

Prior to solving the equations (5.1), (5.2), $(4.45)_{3-5}$, and $(4.45)_{7-12}$, we non-dimensionalize them using the definitions:

$$x \equiv h\bar{x}\,,\ y \equiv h\bar{y}\,,\ u_1(x,y) \equiv U\,\bar{u}_1(\bar{x},\bar{y})\,,$$

$$u_2(x,y) \equiv U\,\bar{u}_2(\bar{x},\bar{y})\,,\ u_f(x) \equiv U\,\bar{u}_f(\bar{x})\,,$$

$$\tilde{u}(y) \equiv U\,\bar{\tilde{u}}(\bar{y})\,,$$

$$T_2(x,y) \equiv (T_s - T_w)\,\bar{T}_2(\bar{x},\bar{y}),\ T_1(x,y) \equiv (T_s - T_w)\,\bar{T}_1(\bar{x},\bar{y})\,,$$

and

$$\dot{m}(x) \equiv \rho_1\, U\, \bar{\dot{m}}(\bar{x})\,. \tag{5.3}$$

The speed U used in (5.3) is of the order of magnitude of the average inlet velocity V_{av}, where

$$V_{av} = \frac{1}{h}\int_0^h \tilde{u}(y)\,dy\,. \tag{5.4}$$

The exact relation of U to V_{av} is specified later in (6.1) after we have chosen a class of inlet vapor velocity profiles $\tilde{u}(y)$. We now non-dimensionalize (5.1)–(5.2), (4.43), (4.44), $(4.45)_{3-5}$, and $(4.45)_{7-12}$ using (5.3) and then drop, for convenience, the overbars on the non-dimensionalized variables introduced in (5.3). The resulting equations are:

$$\dot{m}(x) = \frac{d}{dx} \int_0^{\delta(x)} u_1 (x, y)\, dy = -\left(\frac{\rho_2}{\rho_1}\right) \frac{d}{dx} \int_{\delta(x)}^{1} u_2 (x, y)\, dy \tag{5.5}$$

$$\frac{d}{dx} \int_{\delta(x)}^{1} u_2^2(x, y)dy + \frac{\rho_1}{\rho_2} u_f(x)\dot{m}(x) = \frac{\nu_2}{\nu_1} \frac{1}{Re_1} \left[\frac{\partial u_2}{\partial y} (x, 1) - \frac{\partial u_2}{\partial y} (x, \delta(x))\right] \tag{5.6}$$

$$\dot{m}(x) = \frac{1}{Re_1 Pr_1 Ja} \frac{1}{\delta(x)} , \tag{5.7}$$

$$\frac{\partial u_2}{\partial y} (x, \delta(x)) = \frac{\mu_1}{\mu_2} \frac{u_f(x)}{\delta(x)} , \tag{5.8}$$

$$u_2 (x, \delta(x)) = u_f(x) , \tag{5.9}$$

$$T_2 (x, y) = T_s / (T_s - T_w) \quad \text{for} \quad x > 0 \text{ and } \delta(x) \le y \le 1 , \tag{5.10}$$

$$u_2 (x, 1) = 0 , \tag{5.11}$$

$$v_2 (x, 1) = 0 , \tag{5.12}$$

$$u_2 (0, y) = \tilde{u}(y) \quad \text{for} \quad 0 < y < 1 \text{ with } \tilde{u}(0) = \tilde{u}(1) = 0 , \tag{5.13}$$

$$\delta(0) = 0 , \tag{5.14}$$

and

$$\tilde{u}(0) = u_f(0) = 0 , \tag{5.15}$$

where

$$Re_1 \equiv \frac{\rho_1 U h}{\mu_1}, Pr_1 \equiv \frac{\nu_1}{\alpha_1}, Ja \equiv \frac{h_{fg}}{C_{p_1}(Ts - Tw)}. \quad (5.16)$$

We note that the flow field is determined by the fluid parameters ρ_2/ρ_1, μ_2/μ_1, Pr_1, and the direct control parameters Re_1, $T_s / (T_s - T_w)$, and Ja.

6. The Strategy for an Approximate Solution

We now present a solution scheme which essentially models equations (5.5)–(5.16) by a set of non-linear ordinary differential equations. For this, we choose a representation of the velocity field u_2 (x, y) which incorporates an explicit choice of the variation of the velocity field in the cross-flow direction (y-direction) valid for any admissible inlet velocity profile $\tilde{u}(y)$. Although this method of choosing velocity profiles is common to many integral solution schemes ([19], [14]), the mixed method presented here differs from the usual approaches ([14], [19]) in two important ways:

(i) we use an integral approach for only one of the unknown fields u_2 (x, y), requiring it to satisfy (5.5)-(5.6) instead of $(4.45)_{1-2}$, and we satisfy the rest of the flow field and interface restrictions as in the original differential model (4.43)–(4.45);

(ii) for a chosen representation of u_2 (x, y) , we compare the solution of (5.5)–(5.16) with the solution of (4.43)–(4.45) by defining an error function which measures the difference between the solutions of the two systems and we then compute this measure at every $x > 0$. Therefore, whenever the error function is small at all x, this approach leads to a reliable description of the flow field in Fig. 1.1.

Implementation of the above approach requires the aid of modern computing facilities for symbolic manipulation and numerical integration of non-linear ordinary differential equations. In this spirit, we seek a solution of the flow depicted in Fig. 1.1 for an adequate class of inlet velocity profiles $\tilde{u}(y)$ with a control parameter A. This parameter A can be adjusted to make $\tilde{u}(y)$ approximately resemble many velocity profiles ranging from parabolic to uniform. One such choice of $\tilde{u}(y)$ made in this paper is

$$\frac{u_2(0, y)}{U} \equiv \tilde{u}(y) = 1 - \exp(-Ay) - \exp\left(-A(1-y)\right) + \exp(-A) \qquad (6.1)$$

for $0 \leq y \leq 1$. Note that (6.1) satisfies the restrictions of (5.13) and for large values of A ($A \geq 10$), it approximates uniform inlet flow with rounded corners.

We now choose a representation of $u_2(x, y)$ which assumes a certain y-variation and which has the right number of explicitly occurring functions of x to track the downstream evolution of the profile. This choice is made with the following criteria in mind:

(a) the chosen variation with respect to y should not be very steep at any $\delta(x) < y < 1$ as we do not know the actual variation with respect to y to judge where such sharp variations might occur;

(b) the number of explicitly occurring functions of x in the representation of $u_2(x, y)$ and its values at $y = 1$ and $y = \delta(x)$ should be such that (5.5)–(5.16) transforms into a well-posed initial value problem for a set of non-linear ordinary differential equations; and

(c) it should be possible to track down the evolution of $u_2(x, y)$ from its form $\tilde{u}(y)$ at $x = 0$.

Knowing that we cannot choose a constant or linear variation with respect to y in $u_2(x, y)$ and still satisfy all the restrictions in (5.5)–(5.16), we choose a simple representation of the form

$$u_2(x, y) = b_1(x)\,\tilde{u}(y) + b_2(x)(y-1) + b_3(x)(y^2-1)(1/2)\,, \qquad (6.2)$$

for $x \geq 0$ and $\delta(x) \leq y \leq 1$ with

$$b_1(0) = 1,\ b_2(0) = 0, \text{ and } b_3(0) = 0\,. \qquad (6.3)$$

We see in the next section that substitution of (6.1)–(6.3) in (5.5)–(5.16) leads to a well-posed mathematical problem. To estimate the usefulness of the solution in the form

(6.1)–(6.3), we note that the *true* $u_2(x, y)$ should satisfy the non-dimensionalized equation $(4.45)_2$ given as

$$u_2 \frac{\partial u_2}{\partial x} + v_2 \frac{\partial u_2}{\partial y} - \frac{\nu_2}{\nu_1} \frac{1}{Re_1} \frac{\partial^2 u_2}{\partial y^2} (x, y) \equiv g(x, y) = 0 , \tag{6.4}$$

where $$v_2(x, y) = \int_y^1 \frac{\partial u_2}{\partial x} \, dy.$$

Noting that a solution of the form (6.2) would not, in general, satisfy $g(x, y) \equiv 0$ in (6.4), we introduce

$$\text{error } (x) \equiv \int_{\delta(x)}^1 g^2(x, y) \, dy . \tag{6.5}$$

Now if we find error (x) to be small for most of the values of x of interest, then we can conclude that a solution of (5.5)–(5.16) with the choices (6.1)–(6.3) adequately represents the solution of the original non-linear differential model (4.43)–(4.45). Predictions of such a solution can then be considered to apply to the flow in Fig. 1.1 and its comparison with experiments will establish the value of this solution as well as help us answer questions concerning the validity of the model (4.43)–(4.45).

7. Reduction to a Set of Non-Linear Ordinary Differential Equations

In this section, we substitute our choices (6.1)–(6.3) in (5.5)–(5.16) to arrive at a well-posed mathematical problem leading to a set of coupled non-linear ordinary differential equations in the variables $u_f(x)$, $\delta(x)$, and $b_3(x)$ (see (4.42) and (6.2) respectively for the definitions of $u_f(x)$ and $b_3(x)$). Although the substitution mentioned above is straightforward, it is lengthy and therefore it should only be done on a computer using symbolic manipulations for regular algebra, differentiation, and integration. For the expressions reported in this paper, Maple (a software comparable to MACSYMA) was used. The expressions were found separately by each one of the two authors on two different computers and the results were verified to be identical. Here we outline the underlying logic of the above substitution and the associated manipulations.

First we substitute (6.1) and (6.2) into (5.9) to find

$$b_2(x) \equiv \Psi_1 (\delta(x), u_f(x), b_3(x), b_1(x)), \tag{7.1}$$

where Ψ_1 is defined in (A2.1) of Appendix A2. Next we substitute (6.1), (6.2) and (7.1) into shear condition (5.8) to find

$$b_1(x) = \phi_1 (u_f(x), \delta(x), b_3(x)) , \tag{7.2}$$

where ϕ_1 is defined in (A2.2). Substituting (7.2) in (7.1), we find

$$\begin{aligned} b_2(x) &= \Psi_1 (\delta(x), u_f(x), b_3(x), \phi_1(u_f(x), \delta(x), b_3(x))) \\ &\equiv \phi_2 (\delta(x), u_f(x), b_3(x)) , \end{aligned} \tag{7.3}$$

where ϕ_2 is defined in (A2.4). Substituting (7.2), (7.3), and (6.1) into (6.2), we write

$$u_2 (x, y) \equiv \Phi (\delta(x), u_f(x), b_3(x), y) . \tag{7.4}$$

We now substitute (7.4) and a non-dimensionalized form of (4.43) into (5.5) to find

$$\frac{1}{2} \frac{\rho_1}{\rho_2} \frac{d}{dx} (u_f(x)\, \delta(x)) + \frac{d}{dx}\left[\int_{\delta(x)}^{1} \Phi(\delta(x), u_f(x), b_3(x), y)\, dy \right] = 0 . \tag{7.5}$$

It is easily seen that (7.5) can be rewritten in the form

$$AA11\ (\delta, u_f, b_3) \frac{d\delta}{dx} + AA12\ (\delta, u_f, b_3) \frac{du_f}{dx} + AA13\ (\delta, u_f, b_3) \frac{db_3}{dx} = 0 . \tag{7.6}$$

The non-linear functions AA11, AA12, AA13 are best evaluated using symbolic manipulation on computer and they are defined in the equations (A2.1)–(A2.6) of Appendix A2 with the help of the associated equations (A3.1)–(A3.3) of Appendix A3.

We note that substituting a non-dimensionalized form of (4.43) into the first equality of (5.5) gave

$$\dot{m}(x) = \frac{d}{dx}\left(\frac{1}{2} u_f(x)\, \delta(x)\right). \tag{7.7}$$

Substituting (7.7) in the important interface energy restriction (5.7) gives

$$\frac{d}{dx}\left(\frac{1}{2} u_f(x)\, \delta(x)\right) = \frac{1}{Re_1\, Pr_1\, Ja}\left(\frac{1}{\delta(x)}\right). \tag{7.8}$$

We rewrite (7.8) in a form analogous to (7.6) as

$$AA21\,(\delta, u_f, b_3)\frac{d\delta}{dx} + AA22\,(\delta, u_f, b_3)\frac{du_f}{dx} + AA23\,(\delta, u_f, b_3)\frac{db_3}{dx} = \frac{1}{Re_1\, Pr_1\, Ja}, \tag{7.9}$$

where

$$AA21\,(\delta, u_f, b_3) = \frac{1}{2} u_f(x)\, \delta(x),$$

$$AA22\,(\delta, u_f, b_3) = \frac{1}{2}\delta^2(x),$$

and

$$AA23\,(\delta, u_f, b_3) = 0. \tag{7.10}$$

We now substitute (7.2)–(7.4) and (7.7) in (5.6) to find

$$\frac{d}{dx}\left[\int_{\delta(x)}^{1} \Phi^2\,(\delta(x), u_f(x), b_3(x), y)\, dy\right] + \frac{\rho_1}{\rho_2} u_f(x)\left[\frac{d}{dx}\left(\frac{1}{2} u_f(x)\, \delta(x)\right)\right]$$

$$= \frac{\nu_2}{\nu_1}\frac{1}{Re_1}\left[\frac{\partial u_2}{\partial y}(x, 1) - \frac{\partial u_2}{\partial y}(x, \delta(x))\right]. \tag{7.11}$$

It is easily seen that (7.11) can be rewritten in the form

$$AA31\ (\delta, u_f, b_3)\frac{d\delta}{dx} + AA32\ (\delta, u_f, b_3)\frac{du_f}{dx} + AA33\ (\delta, u_f, b_3)\frac{db_3}{dx}$$

$$= g_2\ (\delta, u_f, b_3)\ . \tag{7.12}$$

The non-linear functions AA31, AA32, AA33, and g_2 are best evaluated using symbolic manipulations on computer and are defined in equations (A2.7)–(A2.8) of Appendix A2 with the help of the associated equations (A3.2)–(A3.5) of Appendix A3.

We now assemble (7.6), (7.9), and (7.12) in the form

$$\begin{bmatrix} AA11 & AA12 & AA13 \\ AA21 & AA22 & AA23 \\ AA31 & AA32 & AA33 \end{bmatrix} \begin{bmatrix} d\delta/dx \\ du_f/dx \\ db_3/dx \end{bmatrix} = \begin{bmatrix} 0 \\ 1/Re_1Pr_1Ja \\ g_2\ (\delta, u_f, b_3) \end{bmatrix}. \tag{7.13}$$

Now (5.14), (5.15), and $(6.3)_3$ suggest that (7.13) should be solved subject to initial conditions

$$\delta(0) = 0\ ,\ u_f(0) = 0\ ,\ b_3\ (0) = 0\ , \tag{7.14}$$

provided the remaining initial conditions

$$b_2(0) = 0\ ,\ b_1(0) = 1\ , \tag{7.15}$$

of $(6.3)_{1-2}$ are satisfied. From the expression of $b_1(x)$ in (A2.2), it follows that if (7.14) and (7.15) are simultaneously true, then

$$\left.\frac{u_f}{\delta}\right|_o \equiv \lim_{x\to 0} \frac{u_f(x)}{\delta(x)} = \frac{\mu_2}{\mu_1} A\ (1 - e^{-A})\ . \tag{7.16}$$

It is found that the expression for $b_2(x)$ in (A2.4) is already consistent with (7.14) and (7.15) being simultaneously true. However, dividing (A2.4) by $\delta(x)$ and then taking the limit of $x\to 0$ gives the condition

$$\left.\frac{b_2}{\delta}\right|_o = A\ (1 - e^{-A})\left[1 - \frac{\mu_2}{\mu_1}\right] - \frac{1}{2}\left.\frac{b_3}{\delta}\right|_o ,$$

where

$$\left.\frac{b_2}{\delta}\right|_o \equiv \lim_{x\to 0} \frac{b_2(x)}{\delta(x)} \text{ and } \left.\frac{b_3}{\delta}\right|_o \equiv \lim_{x\to 0} \frac{b_3(x)}{\delta(x)}. \tag{7.17}$$

There being no additional restrictions on (7.14) and (7.15) being simultaneously true, we require that the solution of (7.13) satisfy (7.14) such that

$$\left.\frac{u_f}{\delta}\right|_o = \frac{\mu_2}{\mu_1} A\,(1 - e^{-A}),$$

and

$$\left.\frac{b_3}{\delta}\right|_o = \lambda, \tag{7.18}$$

where λ is any *finite* real number. However λ is so chosen that the computed value of "error(x)" (defined in (6.4) and (6.5)) is reasonably close to zero for $x > 0$. In fact, for most of the computational results to be reported later, it was found that "error(x)" was small and not very sensitive to the choice of λ in the interval of $0 < \lambda \leq 1$.

We know that numerical integration of (7.13) subject to (7.14) and (7.18) is not possible from $x = 0$ (as terms such as $1/\delta(0)$ are not defined) despite the fact that the actual behavior of the system (7.13) has no real singularity at $x = 0$. Therefore, by choosing a sufficiently small number $\varepsilon_\delta > 0$ and a correspondingly small number for film thickness $\delta(\varepsilon_\delta)$, we rewrite (7.18) as

$$\delta(\varepsilon_\delta) \equiv \delta^*,$$

$$u_f(\varepsilon_\delta) \cong \frac{\mu_2}{\mu_1} A\,(1 - e^{-A})\,\delta^*, \tag{7.19}$$

and

$$b_3(\varepsilon_\delta) \cong \lambda\delta^*.$$

It is now noted that (7.13) subject to (7.19) is a well-posed initial value problem for $x \geq \varepsilon_\delta$ and can be numerically integrated once a reasonable choice for δ^* and λ have been made.

8. Computational Solutions and Prediction of Flow Reversal Phenomena for the Vapor Flow

In order to solve (7.13) subject to the initial conditions (7.19), we further reduce it to the standard form

$$\frac{d\boldsymbol{y}(x)}{dx} = f(\boldsymbol{y}) ,$$

$$\boldsymbol{y}(\varepsilon_\delta) = \boldsymbol{y}^* , \tag{8.1}$$

where

$$\boldsymbol{y}(x) \equiv \begin{bmatrix} \delta(x) \\ u_f(x) \\ b_3(x) \end{bmatrix} , \quad f(\boldsymbol{y}) \equiv \begin{bmatrix} f_1(\delta, u_f, b_3) \\ f_2(\delta, u_f, b_3) \\ f_3(\delta, u_f, b_3) \end{bmatrix}$$

and

$$\boldsymbol{y}^* \equiv \begin{bmatrix} \delta(\varepsilon_\delta) \\ u_f(\varepsilon_\delta) \\ b_3(\varepsilon_\delta) \end{bmatrix} .$$

The function f in (8.1) is easily computed by pre-multiplying (7.13) with the inverse of the coefficient matrix already present on the left side of (7.13). For this it was assumed and computationally verified that the determinant of the coefficient matrix given in (A2.9) is non-zero for $\varepsilon_\delta \leq x \leq M$, where M is some sufficiently large number outside the realm of our interest. The component functions of f thus obtained are defined in (A2.9)-(A2.10). Also note that components of $\boldsymbol{y}^*$ in $(8.1)_2$ are further specified in (7.19).

We use two Runge-Kutta schemes (a fifth and a sixth order) for numerical integration of the standard initial value problem (8.1) and then the solutions from the two schemes are compared and verified to be close to each other. This method is automatically

implemented (see [35]) by a standard IMSL numerical integration scheme called DVERK. The function "error(x)" in (6.4) and (6.5) was numerically evaluated with the help of a symbolic expression for g(x,y) in (6.4) and subsequent numerical integration (a fourth order Simpson's rule) of the right side of (6.5). We now present some of the computational results for typical flow situations involving R-113 and steam. The flow conditions and the corresponding non-dimensional parameters for the two vapors are listed in Table 8.1. Note that all liquid and vapor properties were assumed to be approximately constant in each phase and are evaluated according to the approximations (4.2).

Sample Fluid	Case	Inlet pressure p_∞ (kPa), Saturation temp. Ts (K), Wall temp. Tw (K), inlet vapor flow profile parameter A, and choice of parameter λ	Re_1	Pr_1	Ja	$\frac{\rho_1}{\rho_2}$	$\frac{\mu_1}{\mu_2}$
R-113	1	101.3,320.56,280.57 ,10, 1.	22644	7.18	4.873	202.02	47.92
R-113	2	101.3,320.56,291.56 ,10, 1.	31710	7.18	5.041	202.02	47.92
R-113	3	101.3,320.56,297.56 ,10, 1.	43348	7.18	6.356	202.02	47.92
R-113	4	101.3,320.56,290.57 ,7, 1.	25361.3	7.18	4.873	202.02	47.92
R-113	5	101.3,320.56,291.56 ,7, 1.	35515.5	7.18	5.041	202.02	47.92
R-113	6	101.3,320.56,297.56 ,7, 1.	48550.1	7.18	6.356	202.02	47.92
Steam	7	101.3,373.15,313 ,30, 1.	10000	1.75	8.914	1601.67	23.12
Steam	8	101.3,373.15,313 ,30, 1.	25000	1.75	8.914	1601.67	23.12
Steam	9	101.3,373.15,313 ,30, 1.	100,000	1.75	8.914	1601.67	23.12

Table 8.1. Values of non-dimensional parameters for some typical flow situations.

The choice of flow situations in cases 1-6 of Table 8.1 is made for convenience of comparison with some experimental runs of Christodoulou and Suryanarayana [23]. Their experiments in a duct of rectangular cross-section with condensation on the bottom plate is believed to correspond to the flow geometry in Fig. 1.1. The correspondence between cases in Table 8.1 and the experiments is established by keeping the inlet vapor flow rate in the experiments equal to the inlet flow rate per unit depth in the theoretical model of Fig. 1.1. Since the experiments [23] only report rough measurements of film thickness at a few locations along the duct and overall heat transfer rates across well-defined segments of the bottom plate, we have to assume an inlet velocity profile, the nature of the flow (laminar or turbulent), and we also have to computationally monitor the effect of changing inlet velocity profiles. The cases 1 and 4, as well as cases 2 and 5 and cases 3 and 6, have identical flow rates but different inlet velocity profiles (A=10 and A=7).

The computational runs for each of the cases in Table 8.1 assumes laminar vapor flow. However whether the flow at the inlet section is laminar or turbulent depends both on the inlet Reynold's number and the geometry of the ducts through which the vapor has to flow *prior* to the entrance of the test-section modeling the parallel plate geometry of Fig. 1.1. It is clear that even if the inlet vapor profile was turbulent, rapid loss of momentum flux of the vapor in the flow direction due to an effective suction of vapor at the fluid liquid interface would make the vapor flow laminar at some distance (say L_{tr}) downstream of the inlet. However, it is quite possible that this laminar flow again becomes quite complicated (with condensate turbulence, film break-up etc.) sufficiently further downstream of $x = L_{tr}$. The important information, to be found experimentally, is to obtain an estimate for the critical value of inlet Reynold's number ($Re \equiv V_{av}h/\nu_2$), for any given geometry of ducts leading to the inlet, up to which the transition length L_{tr} mentioned above remains zero or insignificant. For the reported experiments [23], there is no information as to whether the flow in the entrance zone (see Fig. 1.1) is laminar or turbulent. However, because of the condensation phenomena, we believe that a careful design of ducts leading to the inlet section (x=0 in Fig. 1.1) can keep the flow essentially laminar for inlet Reynold's number ($Re \equiv V_{av}h / \nu_2$) as high as 8000 (i.e. for A=10, $Re_1 = 42{,}100$).

To present graphs of relevant physical variables, we assume *laminar* flow for cases in Table 8.1 and define non-dimensional wall heat transfer rate, wall shear stress, and mass condensation rate. For wall heat transfer rate q_w, we write

$$q_w = k_1 \left.\frac{\partial T_1}{\partial y}\right|_{y=0} = k_1 (T_s - T_w)/\delta(x) \equiv h(T_s - T_w) \ ,$$

and

$$Nu_x \equiv \frac{hx}{k_1}, \tag{8.2}$$

then, from (8.2), we find

$$Nu_x \equiv \frac{x}{\delta(x)}. \tag{8.3}$$

The non-dimensional wall shear stress $\tau_w = \mu_1 \partial u_1/\partial y|_{y=0}$ is given by

$$C_f(x) \equiv \frac{\tau_w}{\frac{\rho_1 U^2}{2}} = \frac{2u_f(x)}{(\delta(x)\ Re_1)}. \tag{8.4}$$

We recall that the non-dimensional condensation rate $\dot{m}(x)$ is given by (5.7).

The graphical representations of the computed functions $\delta(x)$, $u_f(x)$, error(x), Nu_x, $C_f(x)$, and $\dot{m}(x)$ are respectfully shown in Figures 8.1-8.6 for the three cases 1-3 of Table 8.1. It is seen from Fig 8.4 that error(x), defined in (6.4) and (6.5), is quite small and therefore the numerical solutions reflect the solution of model equations $(4.45)_{1\text{-}12}$. For brevity, we do not show the plots of $b_1(x)$, $b_2(x)$, $b_3(x)$ etc. as they can be found in Kizilyalli [35]. The velocity profiles $u_2(x, y)$, $v_2(x, y)$ for case-1 in Table 8.1 is shown in Figures 8.7 and 8.8 for different values of x. The nature of downstream evolution of the vapor profile is similar for all of the remaining cases 2-5 in Table 8.1 and these additional graphs can be found in [35]. For Freon-113, it is always found that the x-component of the vapor speed starts losing momentum in the core of the vapor flow regime until there is a flow reversal phenomenon at some distance $x = x_{rev}$ (x_{rev} = 7.04 for case-1). This is *understandable* because condensation demands deficit in

momentum while we still expect that vapor satisfy no slip condition at the wall and at the interface. Since shear should act to resist the vapor flow, we accordingly find correct slopes of $u_2(x, y)$ at the wall and at the interface and a deficit in the core of the velocity profiles in Figure 8.7. Also note that "error(x)" in Fig. 8.3 remains small and it tends to become substantial only for x sufficiently larger than x_{rev}. This means that the negative lobe in the core of the vapor profile $u_2(x, y)$ (Fig. 8.7) for $x > x_{rev} = 7.04$ is a prediction implied by the differential model (4.43)-(4.45) as well. The general trend of $v_2(x, y)$ in Fig. 8.8 is correct but there is a chance of greater error in the values of $v_2(x, y)$ computed through $(6.4)_2$. A physically consistent overall stream line pattern can now be *inferred* from the results as shown in Figures 8.7-8.8 and this leads to the remarkable qualitative inference shown in Figure 1.1. In Figure 1.1, it was assumed that a more accurate differential approach for the solution will lead to small lobes, shown by dotted lines in Fig. 8.8, in the central region of the vapor velocity profile $v_2(x, y)$.

The above results tend to establish that the most important qualitative result is our prediction that a recirculating region forms in the core of the vapor (Freon-113) flow (Fig. 1.1) beyond $x > x_{rev}$ where x_{rev} increases with increasing Reynold's number. This phenomenon is important because the flow would eventually lead to a point, some distance downstream of x_{rev}, where the vapor and film would lose stability and more complex flows would initiate. However, depending on fluid parameters and inlet velocity profile, recirculating zones may form at different locations in the vapor flow. For example, at Re = 10,000 and $x_{rev} = 3.46$ for steam (case 7 in Table 8.1), recirculating zone seems to form near the upper plate (see Figure 8.9). These identifications establish the need for additional computational and experimental efforts towards establishing these flow phenomena.

For the same flow rate, the effect of a change in the inlet velocity profile on the film thickness profile and the point of flow reversal is shown in Figure 8.10. It is found that the effect is small for moderate changes in the inlet velocity profile $\tilde{u}$ (y) as long as all the flows at the inlet are laminar.

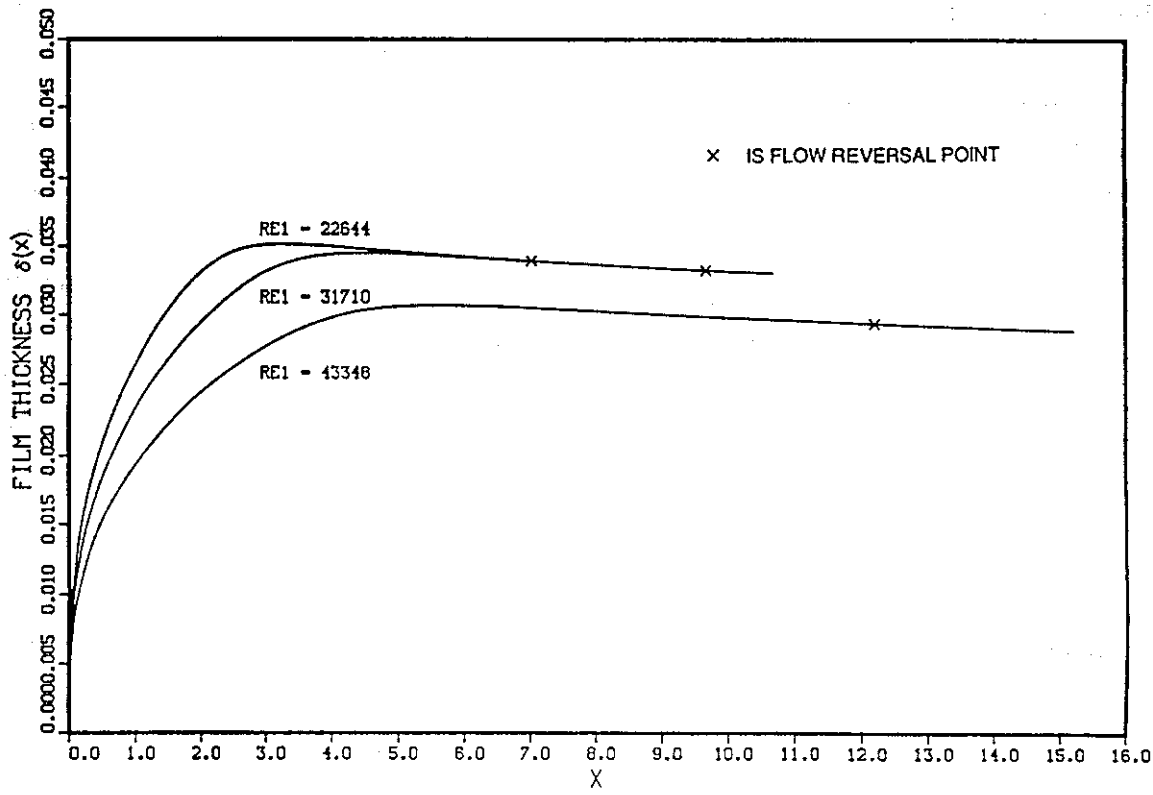

Figure 8.1: The $\delta(x)$ vs x curves are for cases 1-3 in Table 8.1. Note the tendency of the film thickness to reach an approximately constant value. With increasing speed, (Reynolds number), we typically obtain thinner condensate and higher local heat transfer rates. The flow reversal distances x_{rev} in each case is marked by 'x' symbols and these values are obtained from corresponding graphs of u_2 (x, y) (see Figure 8.7)

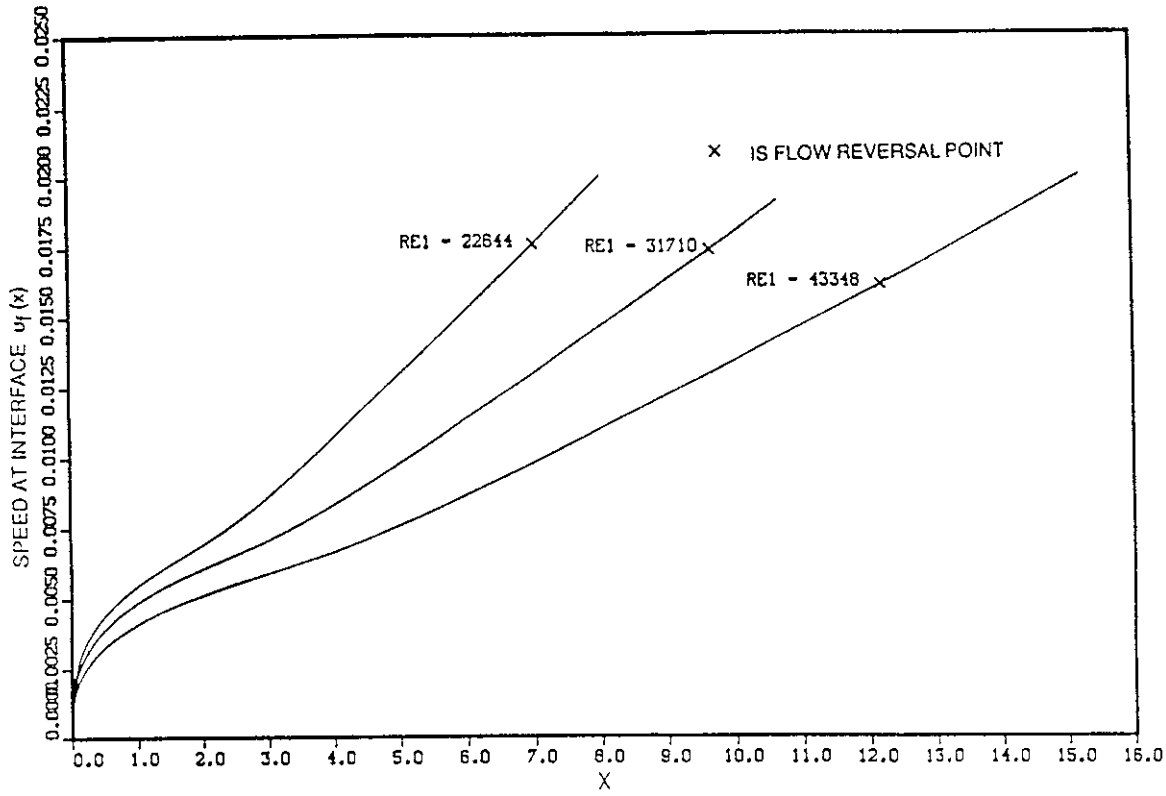

Figure 8.2: The speed of the fluid at the interface u_f (x) tends to increase with x for cases 1-3 of Freon-113. Again the flow reversal points x_{rev} for each case is marked by 'x'. The three plots correspond to cases 1-3 of Table 8.1.

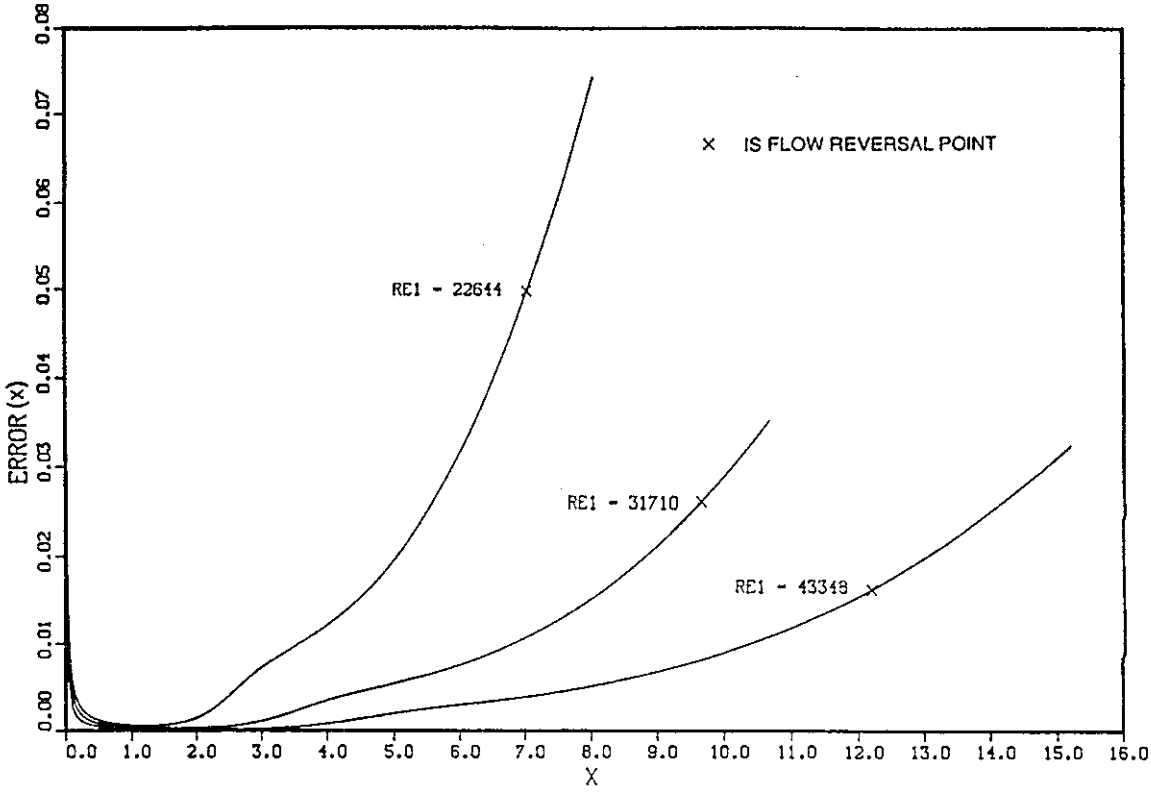

Figure 8.3: These plots indicate that error(x) remains acceptably small for most values of x of interest. The tendency of error to increase beyond $x > x_{rev}$ is expected because the chosen representation of $u_2(x, y)$ is not likely to give good results in the more complex recirculating zones in this region. The three plots correspond to cases 1-3 of Table 8.1.

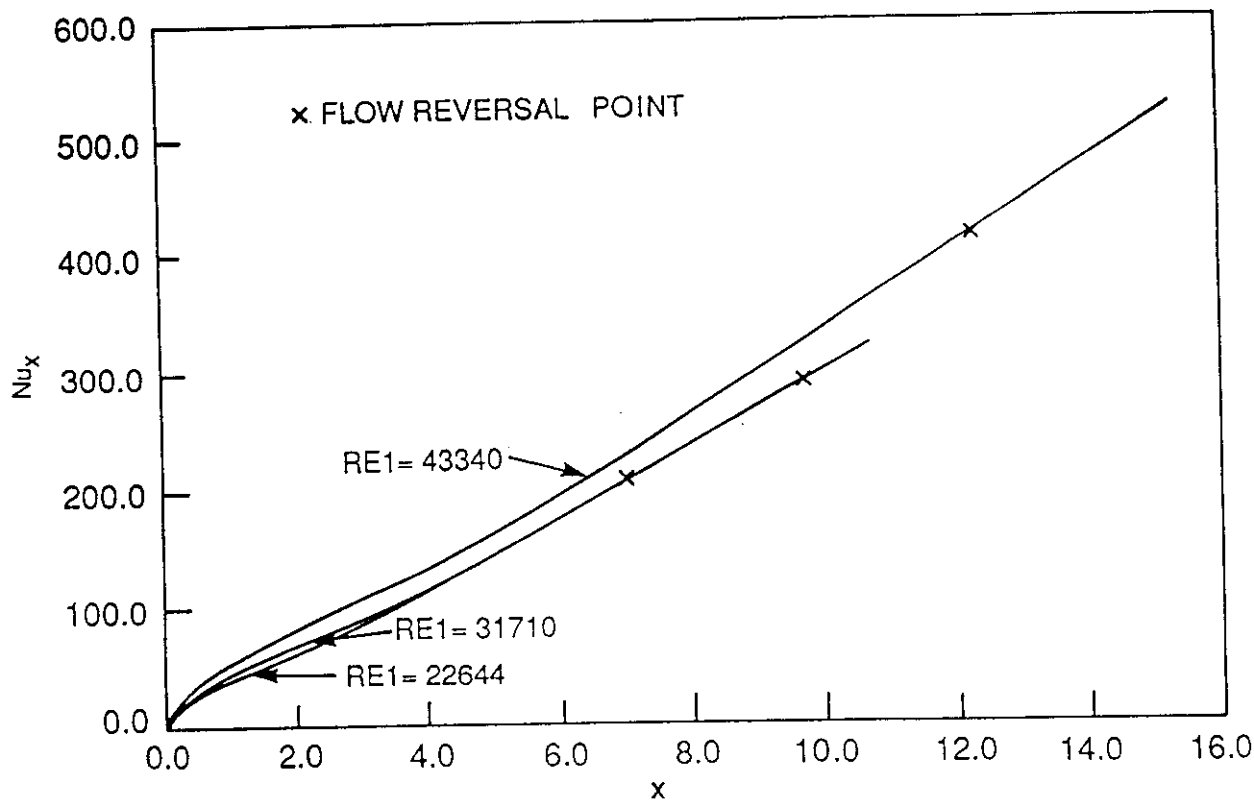

Figure 8.4: The non-dimensional Nusselt number defined in (8.3) tends to increase with x. The three plots correspond to cases 1-3 of Table 8.1.

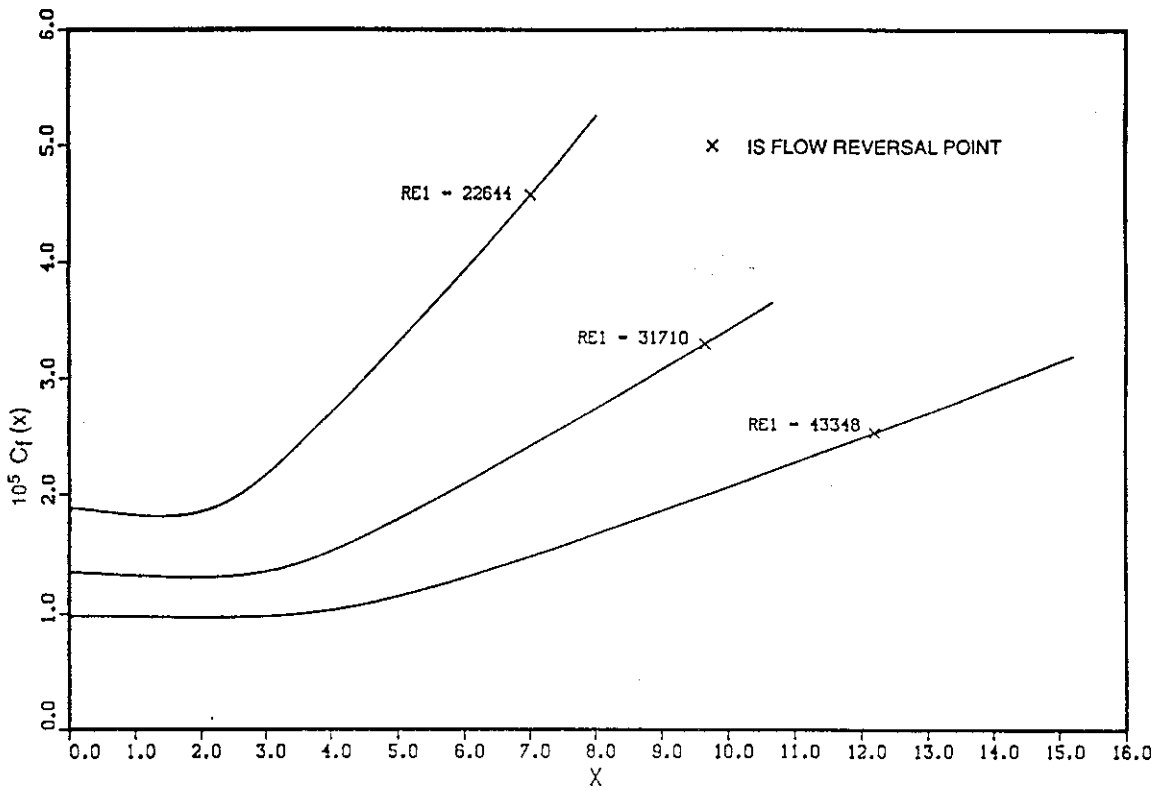

FIGURE 8.5: The non-dimensional friction C_f (x) at the bottom plate is given by (8.4) and are plotted here for cases 1-3 of Table 8.1.

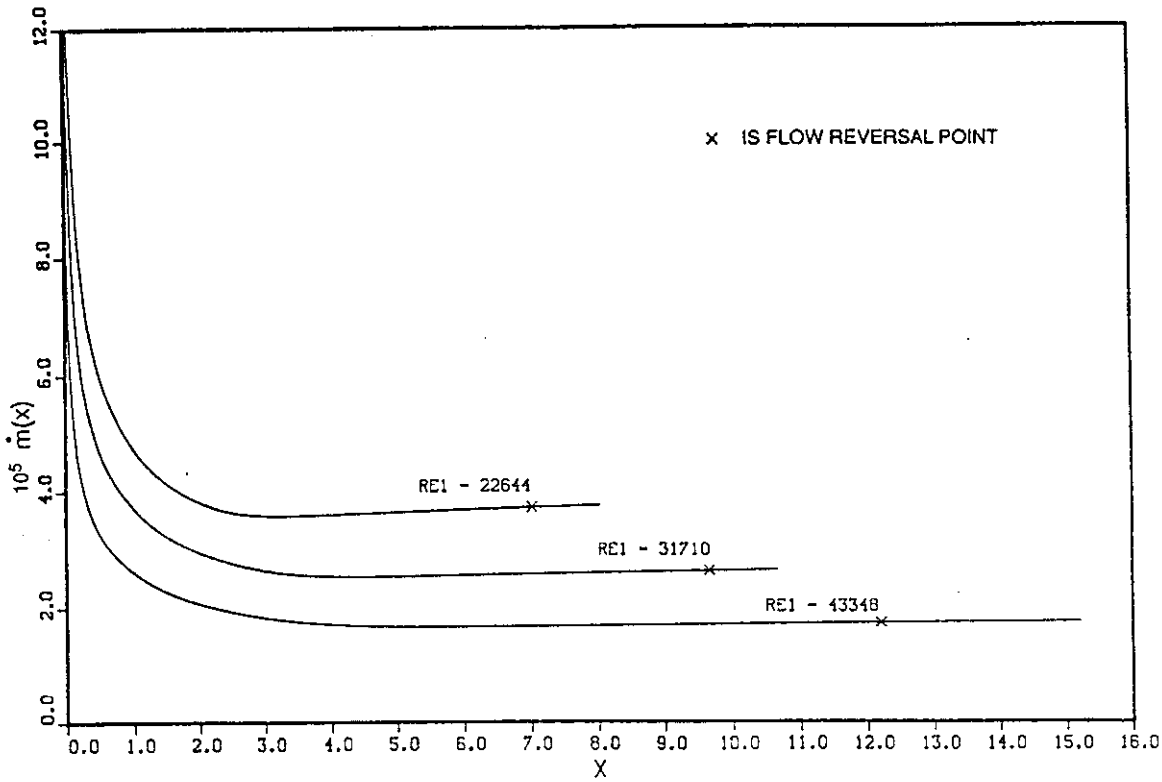

Figure 8.6: The condensation rate $\dot{m}(x)$ is relatively higher near the leading edge (high $d\delta/dx$) and it tends to flatten out away from the leading edge. Here $\dot{m}(x)$, as given by (5.7), is plotted for the cases 1-3 in Table 8.1.

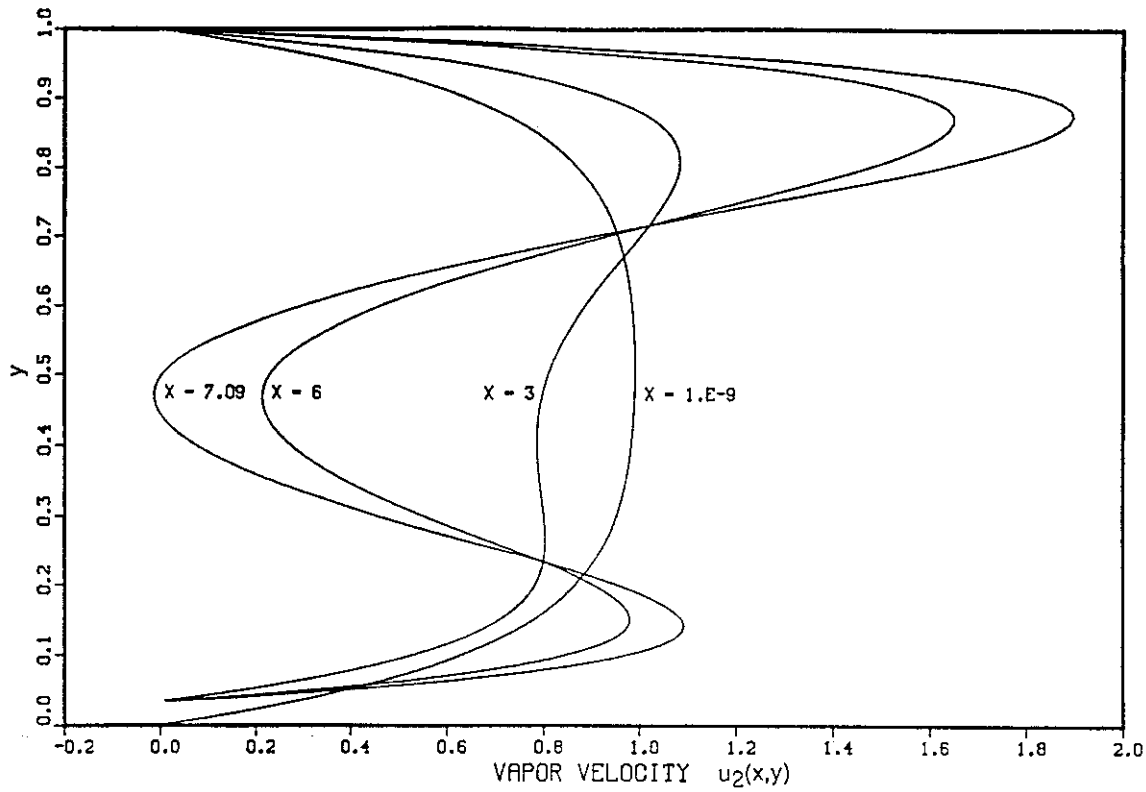

Figure 8.7: The vapor velocity profile u_2 (x, y) is plotted here for case-1 in Table 8.1. The plots are with respect to y ($\delta(x) \leq y \leq 1$) for different values of x. It is clear that the inlet profile ($x = 10^{-9} \cong 0$) quickly starts losing its momentum in the core and at x = 7.04, the vapor velocity u_2 has a value of zero at y between 0.4 and 0.5. Beyond this distance $x_{rev} = 7.04$, the flow reverses and we have a zone in the core of the vapor flow where the vapor velocity is negative. Since the value of error(x) is still small at $x = x_{rev}$, we *infer* the existence of recirculating zones for $x > x_{rev}$.

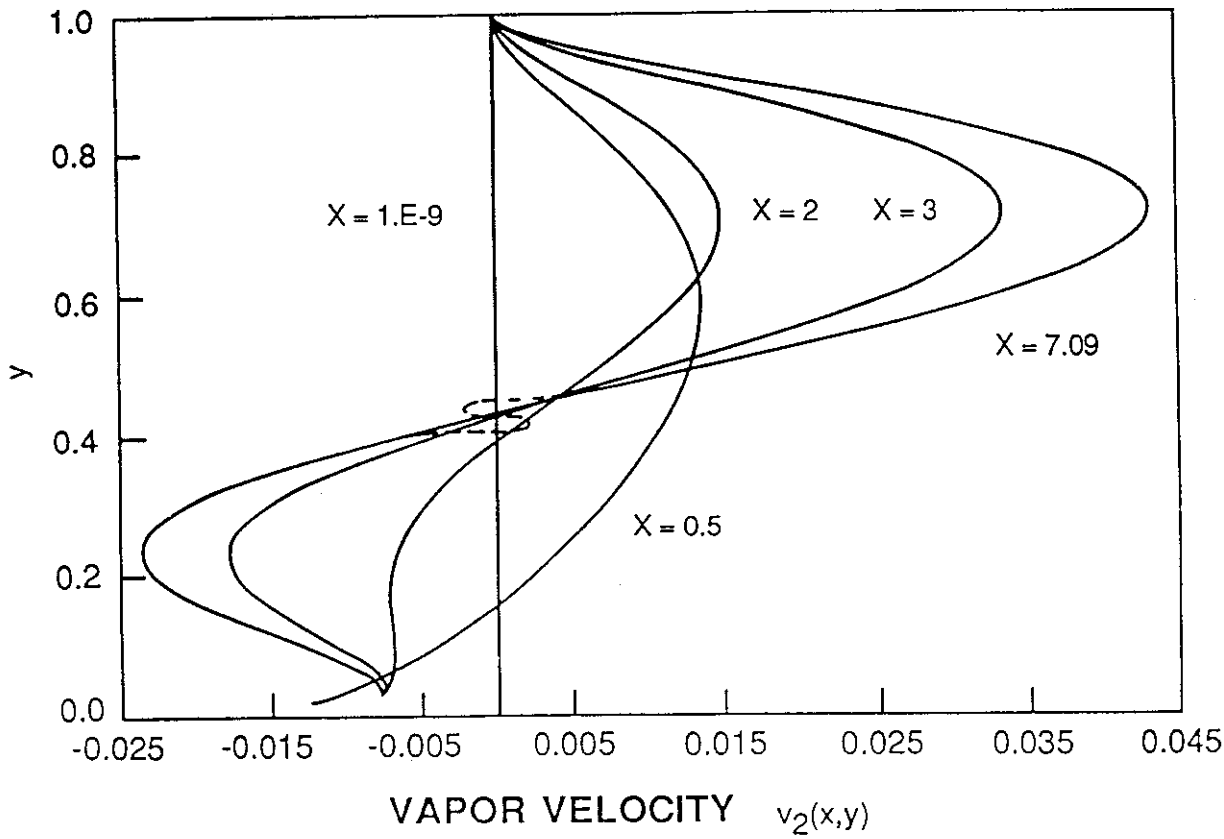

Figure 8.8: The vapor velocity component v_2 (x, y) is plotted here for case-1 in Table 8.1. The plots are with respect to y for different values of x and we see that the vapor is directed towards the upper plate in the upper region and towards the lower plate in the lower region. We expect that at $x > x_{rev}$, the v_2 (x, y) component will develop some tiny lobes as shown by dotted lines in the profile for x = 7.09. Our approximate method is unable to pick the existence of these lobes but its existence is *inferred* from the point of overall consistency of streamline patterns (see Figure 1.1).

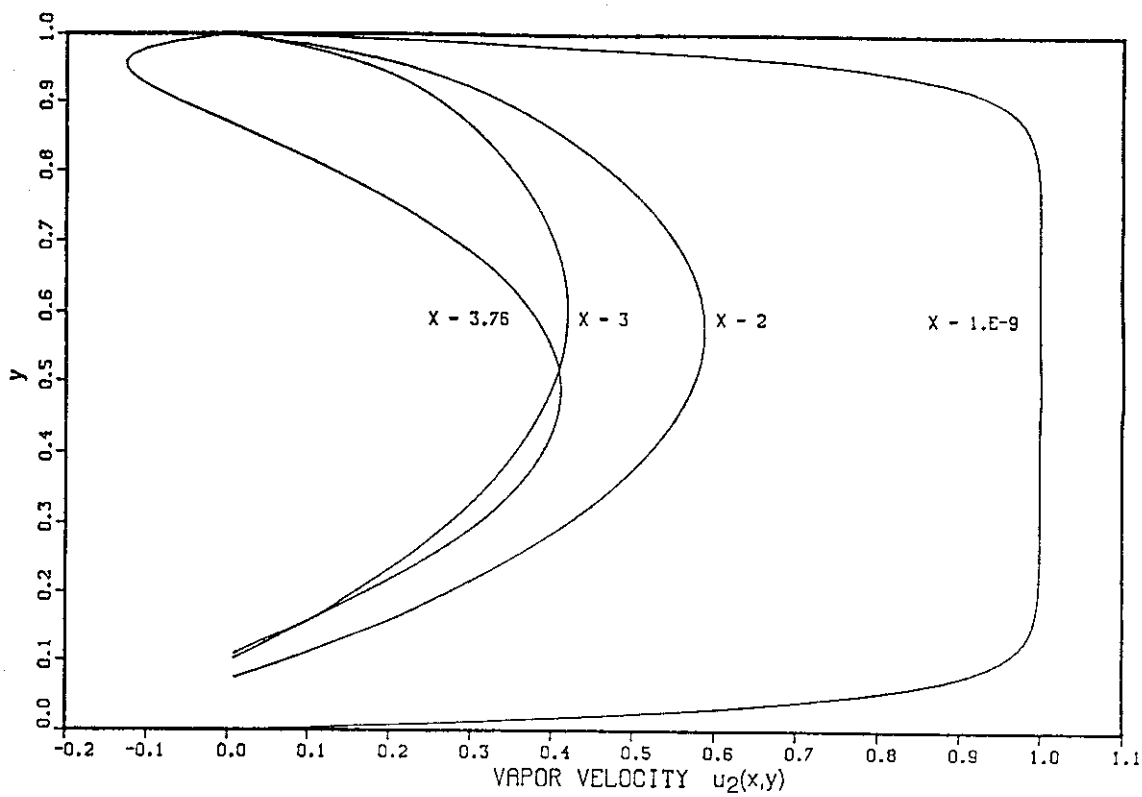

Figure 8.9: The u_2 (x, y) component for flow of steam in case-7 of Table 8.1 is plotted here with respect to y for different values of x. Computations indicated that for $x > x_{rev} = 3.46$, the vapor velocity became negative near the upper plate. This may mean that the shear restriction for steam is not very significant at the interface and therefore recirculating zones form near the upper plate. Note also that the inlet vapor velocity profile is nearly uniform.

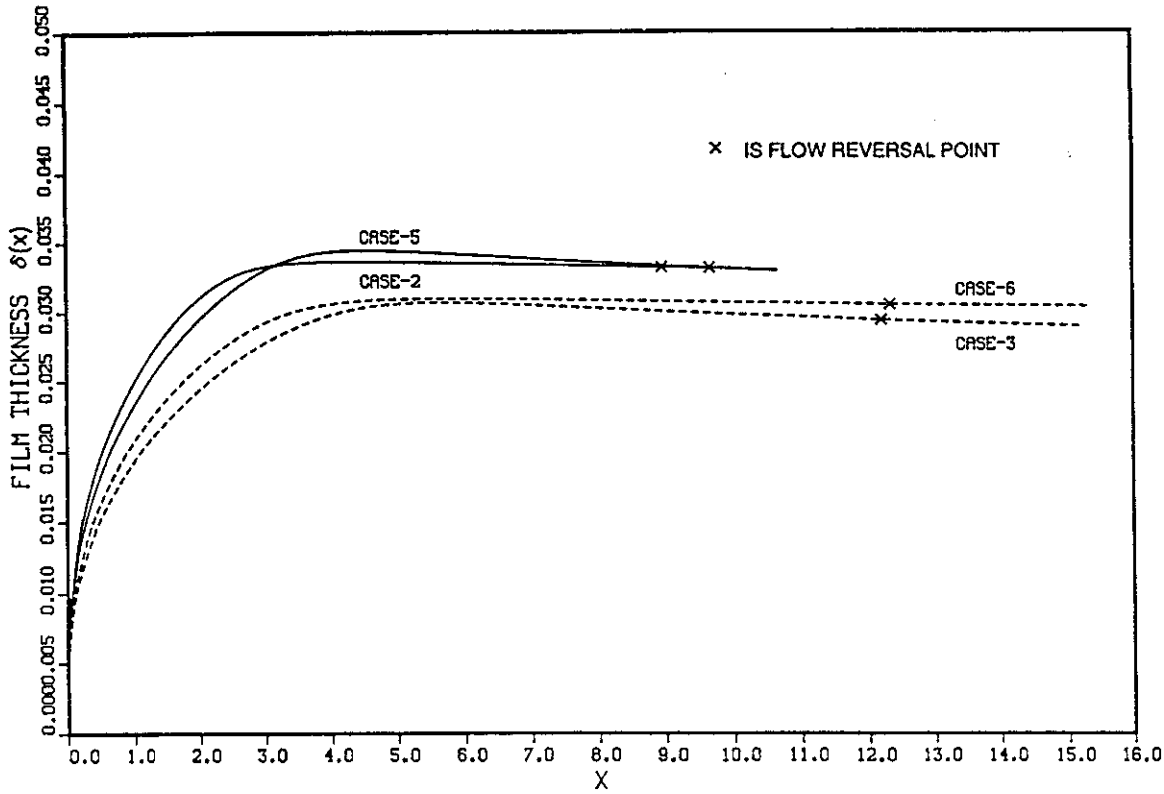

Figure 8.10: Note that cases 2 and 5 in Table 8.1 correspond to the same vapor flow rate but different inlet profiles (A = 10 and A = 7 respectively). Cases 6 and 3 of Table 8.1 are also analogous. The $\delta(x)$ versus x for these two pairs of cases indicate that film thickness profiles and reversal distances (x_{rev}) are affected only slightly by *moderate* changes in *laminar* inlet profiles.

9. Comparisons with a relevant experiment and conclusions.

Although there is no experiment known to us which accurately models the flow in Fig. 1.1, the experiments reported in [23] come quite close to modeling flow between parallel plates. The differences between this theory and the experiments [23] are (i) that they use a duct of rectangular cross-section (0.025 m high and 0.04 m wide); (ii) that their temperatures of the bottom plate varies by about 5-10 °C over the length (0.924 m) of the plate; (iii) that their inlet vapor has 5-7 °C superheat over the saturation temperature, and (iv) that the design of their experimental set up does not provide for measurements to insure that the vapor flow is *laminar* when it enters the test section.

For comparison purposes, we take the flow rate (per unit depth in Fig. 1.1) to be the same as their [23] inlet volume flow rate in the duct and the wall temperature T_w to be the average temperature of the bottom plate in the experiments [23]. We also know, from the effects of superheat found in the flat plate theory [15], that the 5-7° C superheat in the experiments [23] should not have more than 1-2% effect on the values of film thickness and overall heat transfer rates. Under these approximating assumptions, the first three differences mentioned in the previous paragraph, should not cause a substantial difference between the numerical predictions of this paper and the reported experimental results [23]. However, perhaps partially because of the fourth reason mentioned in the previous paragraph, we find that our theory overpredicts film thickness and therefore underpredicts heat transfer rates by a substantial amount in comparison to any relevant run in the experiment [23]. The differences between film thickness measurements and predictions, for case-3 in Table 8.1 corresponding to run 6 in experiments [23], is illustrated in Figure 9.1. Note that the theory, in Fig. 9.1, overpredicts film thickness by a factor of 2 to $2\frac{1}{2}$. However, we observe that the film thickness in Fig. 8.1 is nearly constant over most of the bottom plate and this is in *qualitative* agreement with the experiments [23]. We now try to reconcile the quantitative differences between theory and experiments.

Note that scalings of section 4, except for $(4.7)_2$, are standard (see boundary layer approximations [34]) and they are not valid only in a *very small* region near the leading edge. Similarly the approximation (4.24) of (4.23) does not lead to any significant error as can be seen by the following analysis. In $(4.29)_2$ for $I = 1$, we can still ignore inertia, but we find that the order of magnitude of pressure force, due to (4.23), is given by

$$O\left(-\frac{\partial p_1}{\partial x}\right) \sim 2\dot{m}\frac{d\dot{m}}{dx}\left(\frac{1}{\rho_2} - \frac{1}{\rho_1}\right), \tag{9.1}$$

and the order of magnitude of viscous force is given by

$$O\left(\mu_1 \frac{\partial^2 u_1}{\partial y^2}\right) \sim \mu_1 \frac{U}{\delta^2} . \tag{9.2}$$

Using $(4.45)_5$ for $\dot{m}$ and approximating

$$O\left(\frac{d\delta}{dx}\right) \sim \frac{\delta(x)}{x} ,$$

we find that the ratio of the pressure force (due to condensation) and viscous force in the liquid condensate near the leading edge is

$$\left(\frac{Ja}{Pr_1}\right)^2 \left(\frac{\rho_1}{\rho_2} - 1\right) \frac{1}{Re_x} , \tag{9.3}$$

where $Re_x \equiv \rho_1 Ux / \mu_1$.

It is easily verified that the quantity in (9.3), for most flows, is very small for $x \geq \bar{\varepsilon}$ where $\bar{\varepsilon}/h$ is typically a very small number . These discussion establish that the deficiencies in the differential model (4.43)-(4.45) can only affect the choice of initial conditions in (7.19) in a small way and therefore can, at most, lead to small errors (say 10-15%) and should not lead to errors of the order of magnitude in Figure 9.1. The assumption $(4.7)_2$ *may* lead to substantial error if the contribution of viscous stress $\mu_2 \partial v_2/\partial x$ in the expression for $\tau_f(x)$ is important over $0 \leq x/h \leq 2$. However, since in Figure 8.6, dm/dx and therefore $\mu_2 \partial v_2/\partial x$ at the interface is nearly zero for $x \geq 1$, it is unlikely that this would lead to very large errors (say larger than 20-30%). The major quantitative difference in Figure 9.1, in our opinion, is due to the fact that the reported experiments [23] involve *turbulent* vapor flow at the inlet while our model here is for *laminar* flows.

In fact, in their experiment [23], the vapor flows in long pipes (1/4 to 1/2 inch diameter) at Reynold's number of the order of 10,000 (» 2300) and this turbulent flow enters the test-section after passing through a very small diffuser (about 4" in diameter and 10" long). This means that the vapor flow is turbulent and the distance L_{tr} needed for laminarization (see section 8 before) may be significant. Our model does not apply over this zone ($0 \leq x \leq L_{tr}$) as turbulent shear stresses and heat fluxes dominate to make the condensate layer substantially thinner. However the experimental flow should eventually become laminar and this *perhaps* explains the qualitative similarity between theory and experiments. In fact, in a careful experiment, if we are given the film thickness $\delta(x)$, the interfacial speed $u_f(x)$, and some average vapor speed (this will give us $b_3(x)$) at an $x = x^*$ larger than 3 and L_{tr}/h (insuring that both $(4.7)_2$ and the assumption of laminarity is satisfied), then (7.19) can be replaced by experimental initial values at $x = x^*$ and we can expect an excellent quantitative and qualitative

agreement with experiments. This type of prediction, whenever such experimental data is available ,would lead to predictions as shown by the dotted lines in Figure 9.1.

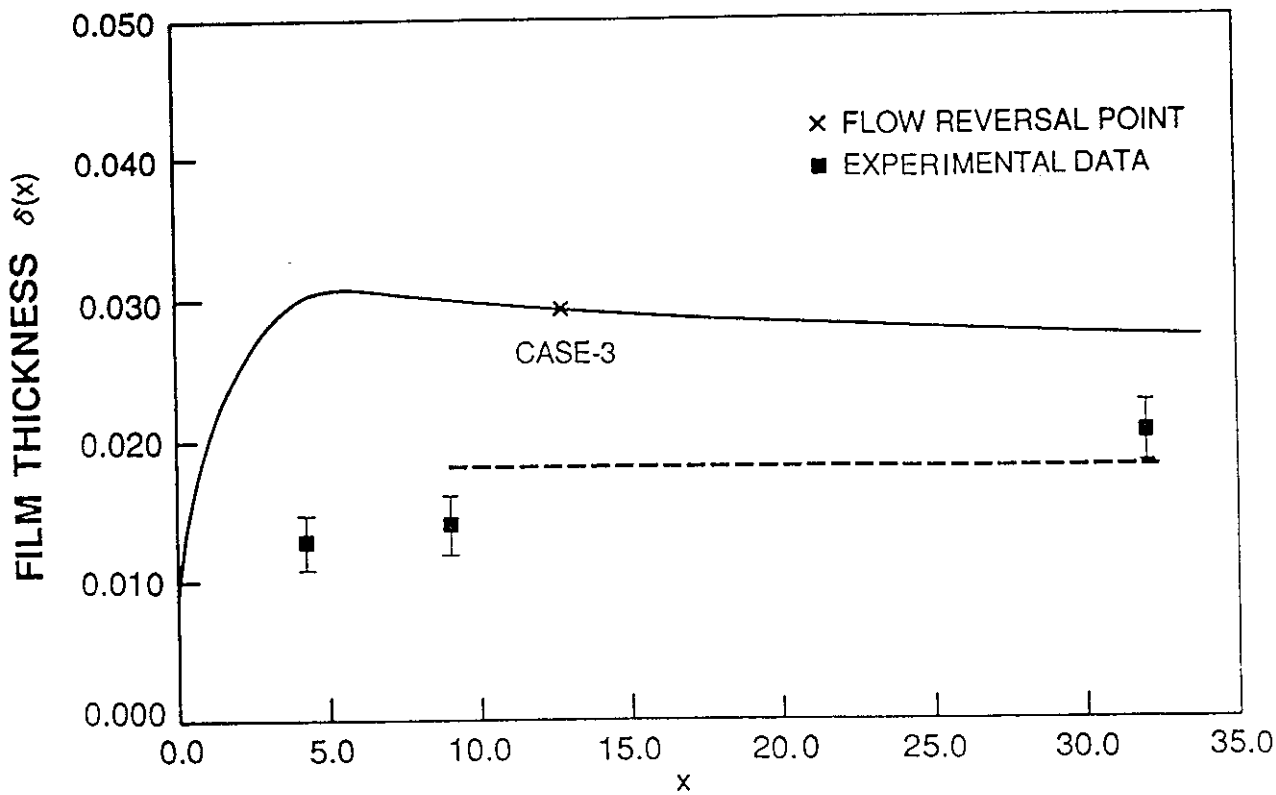

Figure 9.1: The prediction of $\delta(x)$ for case-3 in Table 8.1 is compared with some experimental measurements of film thickness at x = 4, x=9, and x=32. We observe that the theoretical prediction is 2 to 2½ times higher. This is due to the fact that the experiment corresponds to *turbulent* vapor flows and slightly due to the fact that theory has some inaccuracies in $0 \leq x \leq 2$. The dashed line corresponds to expected theoretical predictions when sufficient experimentally measured information is available at some suitable $x = x^*$.

Acknowledgement

Institute of Mathematics and its Applications at the

This research was supported partially by NASA-Lewis grant NAG 3-711 and by an NSF visiting grant at the University of Minnesota. Computational aspects of this paper also forms a part of M.S. thesis of Y. Kizilyalli.

We also thank Prof. N. V. Suryanaryana (Michigan Technological University) for sharing information on his ongoing experiments and discussions leading to our formulation and study of this problem.

Appendix A1.

For the flow between parallel plates satisfying (4.1)-(4.4) the interface conditions (3.6)-(3.13) are written here in more detail. The kinematic conditions (3.6), for $I(\mathbf{x},t)=y-\delta(x)=0$ gives

$$\mathbf{v}_s \cdot \mathbf{n} = 0 \tag{A1.1}$$

Note that with $\mathbf{n} = [-\delta'\mathbf{i} + \mathbf{j}]/\sqrt{1+(\delta')^2}$ and $\mathbf{t} = [\mathbf{i} + \delta'\mathbf{j}]/\sqrt{1+(\delta')^2}$ the condition (3.7) reduces to

$$\left\{\frac{1}{\sqrt{1+(\delta')^2}}\right\}\left\{u_1(x,\delta(x)) + \frac{d\delta}{dx}v_1(x,\delta(x))\right\}$$
$$= \frac{1}{\sqrt{1+(\delta')^2}}\left\{u_2(x,\delta(x)) + \frac{d\delta}{dx}v_2(x,\delta(x))\right\} \tag{A1.2}$$

The interface mass balance condition (3.8) reduces to

$$\dot{m}(x) = \frac{\rho_1}{\sqrt{1+(\delta')^2}}\left[u_1(x,\delta(x))\frac{d\delta}{dx} - v_1(x,\delta(x))\right]$$
$$= \frac{\rho_2}{\sqrt{1+(\delta')^2}}\left[u_2(x,\delta(x))\frac{d\delta}{dx} - v_2(x,\delta(x))\right] \tag{A1.3}$$

For the evaluation of terms like $\nabla_s\sigma$, $\nabla_s\cdot(\sigma\mathbf{v}_t\mathbf{t})$, $\nabla_s\cdot\mathbf{n}$, one can use formulas on p. 53 and p. 223 of Weatherburn [31]. We find, for $\sigma=\sigma(x)$,

$$\nabla_s\sigma = \frac{d\sigma}{dx}\mathbf{t}, \quad \nabla_s\cdot\mathbf{n} = \left\{\frac{-1}{\left(1+\delta'(x)^2\right)^{3/2}}\right\}\delta''(x),$$

and

$$\nabla_s\cdot(\sigma\mathbf{v}_t\mathbf{t}) = \frac{d}{dx}\left[\left(\frac{\sigma}{(1+\delta'(x)^2)}\right)\left\{u_1(x,\delta(x)) + \delta'(x)v_1(x,\delta(x))\right\}\right]$$
$$+\left[\left(\frac{\sigma\delta'\delta''}{(1+\delta'^2)^2}\right)\left\{u_1(x,\delta(x)) + \delta'(x)v_1(x,\delta(x))\right\}\right] \tag{A1.4}$$

The interface momentum condition (3.9) in the normal direction with the use of (3.1), (3.8), and (4.1).

$$\dot{m}(x)^2\{1/\rho_2 - 1/\rho_1\} + \{p_2(x,\delta(x)) - p_1(x,\delta(x))\}$$
$$+\frac{2}{1+\delta'^2}\left[\left(\mu_1\frac{\partial u_1}{\partial x}\Big|^i\right)\delta'(x)^2 - \mu_1\left(\frac{\partial u_1}{\partial y}+\frac{\partial v_1}{\partial x}\right)\Big|^i\ \delta'(x) + \mu_1\frac{\partial v_1}{\partial y}\Big|^i\right]$$
$$-\frac{2}{1+\delta'^2}\left[\left(\mu_2\frac{\partial u_2}{\partial x}\Big|^i\right)\delta'(x)^2 - \mu_2\left(\frac{\partial u_2}{\partial y}+\frac{\partial v_2}{\partial x}\right)\Big|^i\ \delta'(x) + \mu_2\frac{\partial v_2}{\partial y}\Big|^i\right]$$
$$-\sigma\delta''(x)/\{1+\delta'(x)^2\}^{3/2} = 0\ . \qquad \text{(A1.5)}$$

The same condition (3.9) in the tangential direction with the use of (3.1), (3.8), and (4.1) gives

$$\left(\frac{1}{1+\delta'^2}\right)\left[\mu_1\left(\frac{\partial u_1}{\partial y}+\frac{\partial v_1}{\partial x}\right)\Big|^i - \delta'\left\{2\mu_1\frac{\partial u_1}{\partial x}\Big|^i + \mu_1\delta'\left(\frac{\partial u_1}{\partial y}+\frac{\partial v_1}{\partial x}\right)\Big|^i - 2\mu_1\frac{\partial v_1}{\partial y}\Big|^i\right\}\right]$$
$$-\left(\frac{1}{1+\delta'^2}\right)\left[\mu_2\left(\frac{\partial u_2}{\partial y}+\frac{\partial v_2}{\partial x}\right)\Big|^i - \delta'\left\{2\mu_2\frac{\partial u_2}{\partial x}\Big|^i + \mu_2\delta'\left(\frac{\partial u_2}{\partial y}+\frac{\partial v_2}{\partial x}\right)\Big|^i - 2\mu_2\frac{\partial v_2}{\partial y}\Big|^i\right\}\right]$$
$$-\frac{d\sigma}{dx} = 0\ . \qquad \text{(A1.6)}$$

The interface energy equation (3.11) is rewritten with the help of (3.1), (3.2), (3.7), and (4.1)-(4.4). This gives

$$\left[\dot{m}(x)\{h_1|^i - h_2|^i\} + \dot{m}\left\{\frac{1}{2}\left|\mathbf{v}_1^i - \mathbf{v}_s\right|^2 - \frac{1}{2}\left|\mathbf{v}_2^i - \mathbf{v}_s\right|^2\right\} + \left\{\mathbf{S}_1^i\mathbf{n}\cdot(\mathbf{v}_1^i - \mathbf{v}_s) - \mathbf{S}_2^i\mathbf{n}\cdot(\mathbf{v}_2^i - \mathbf{v}_s)\right\}\right.$$
$$+\left(\frac{1}{\sqrt{1+\delta'^2}}\right)\left\{k_1\left(\frac{\partial T_1}{\partial y}\Big|^i - \delta'\frac{\partial T_1}{\partial x}\Big|^i\right) - k_2\left(\frac{\partial T_2}{\partial y}\Big|^i - \delta'\frac{\partial T_2^i}{\partial x}\Big|\right)\right\}$$
$$\left.+\left\{-\frac{\partial}{\partial x}\left(\frac{\sigma(u_1|^i + \delta' v_1|^i)}{\sqrt{1+\delta'^2}} - \frac{\sigma\delta'\delta''(u_1|^i + \delta' v_1|^i)}{(1+\delta'^2)^2} + \frac{d\sigma}{dx}v_t\right)\right\}\right] = 0\ . \qquad \text{(A1.7)}$$

In (A1.5)-(A1.7), $\dot{m}(x)$ is given by (A1.3) and the superscript 'i' on the right side of some of the terms indicates interfacial values. As it is straightforward to write the kinetic energy and viscous working terms in (A1.7) in component form, we leave (A1.7) in its current form for brevity. The condition (3.12) is rewritten, for I=1 or 2, as

$$T_I(x,\delta(x)) = T_s(p_I(x,\delta(x)) = T_s\ . \qquad \text{(A1.8)}$$

The condition (3.13) needs no further simplification.

Appendix A.2

Following the steps at (7.1), we find

$$b_2(x) \equiv \Psi_1(\delta(x),u_f(x),b_3(x),b_1(x))$$
$$= \frac{u_f(x)}{\delta(x)-1} - b_1(x)\ \text{expr1}(\delta) - b_3(x)\ \frac{\delta(x)+1}{2}, \qquad \text{(A2.1)}$$

where $\text{expr1}(\delta) \equiv (1-\exp(-A\delta)-\exp(-A(1-\delta))+\exp(-A))(1/(\delta-1))$. Following the steps leading to (7.2), we find

$$b_1(x) \equiv \phi_1(u_f(x),\delta(x),b_3(x))$$
$$= \frac{1}{\text{expr3}(\delta)-\text{expr1}(\delta)}\left[\text{expr2}(\delta)u_f(x) + \left(\frac{b_3(x)}{2}\right)(1-\delta(x))\right], \qquad \text{(A2.2)}$$

where expr1 was defined following (A2.1) and we have

$$\text{expr2}(\delta) \equiv \left(\frac{1}{\delta(\delta-1)}\right)\left(\left(\frac{\mu_1}{\mu_2}\right)(\delta-1)-\delta\right),$$

$$\text{expr3}(\delta) \equiv A\exp(-A\delta) - A\exp(-A(1-\delta)) . \qquad \text{(A2.3)}$$

Following the steps leading to (7.3), we find

$$b_2(x) \equiv \phi_2(u_f(x),\delta(x),b_3(x))$$
$$= \frac{u_f(x)}{\delta(x)-1} - \frac{\text{expr1}(\delta)}{(\text{expr3}(\delta)-\text{expr1}\ (\delta))}\left[\text{expr2}(\delta)u_f(x) + \frac{b_3(x)}{2}(1-\delta(x))\right]$$
$$- b_3(x)\ \frac{(\delta(x)+1)}{2}. \qquad \text{(A2.4)}$$

We now implement the steps outlined in (7.4)-(7.6) by introducing the following definitions

$$I_1 \equiv I_1(u_f,\delta,b_3) \equiv \int_{\delta(x)}^{1} \Phi(u_f(x),\delta(x),b_3(x),y)\ dy . \qquad \text{(A2.5)}$$

Now the functions AA11,AA12,AA13 in (7.6) are given by

$$AA11(u_f,\delta,b_3) \equiv \left[\frac{\partial I_1}{\partial \delta} + \frac{\partial I_1}{\partial b_1}\frac{\partial b_1}{\partial \delta} + \frac{\partial I_1}{\partial b_2}\frac{\partial b_2}{\partial \delta} + \frac{1}{2}\frac{\rho_1}{\rho_2}u_f\right],$$

$$AA12(u_f,\delta,b_3) \equiv \left[\frac{\partial I_1}{\partial u_f} + \frac{\partial I_1}{\partial b_1}\frac{\partial b_1}{\partial u_f} + \frac{\partial I_1}{\partial b_2}\frac{\partial b_2}{\partial u_f} + \frac{1}{2}\frac{\rho_1}{\rho_2}\delta\right],$$

$$AA13(u_f,\delta,b_3) \equiv \left[\frac{\partial I_1}{\partial b_3} + \frac{\partial I_1}{\partial b_1}\frac{\partial b_1}{\partial b_3} + \frac{\partial I_1}{\partial b_2}\frac{\partial b_2}{\partial b_3}\right]. \qquad (A2.6)$$

The partial derivatives occurring in (A2.6) are defined in equations (A3.1)-(A3.3) of Appendix A3.

Introducing the following definition:

$$I_2 \equiv I_2(u_f,\delta,b_3) \equiv \int_{\delta(x)}^{1} \Phi^2(u_f(x),\delta(x),b_3(x),y)\, dy \ , \qquad (A2.7)$$

we can now relate (7.11) to (7.12) using the following definitions

$$AA31(u_f,\delta,b_3) = \left[\frac{\partial I_2}{\partial \delta} + \frac{\partial I_2}{\partial b_1}\frac{\partial b_1}{\partial \delta} + \frac{\partial I_2}{\partial b_2}\frac{\partial b_2}{\partial \delta} + \frac{1}{2}\frac{\rho_1}{\rho_2}u_f^2\right],$$

$$AA32(u_f,\delta,b_3) = \left[\frac{\partial I_2}{\partial u_f} + \frac{\partial I_2}{\partial b_1}\frac{\partial b_1}{\partial u_f} + \frac{\partial I_2}{\partial b_2}\frac{\partial b_2}{\partial u_f} + \frac{1}{2}\frac{\rho_1}{\rho_2}u_f\,\delta\right],$$

$$AA33(u_f,\delta,b_3) = \left[\frac{\partial I_2}{\partial b_3} + \frac{\partial I_2}{\partial b_1}\frac{\partial b_1}{\partial b_3} + \frac{\partial I_2}{\partial b_2}\frac{\partial b_2}{\partial b_3}\right], \qquad (A2.8)$$

and

$$g_2(\delta,u_f,b_3) = \frac{\nu_2}{\nu_1}\frac{1}{Re_1}\left[b_1(x)A\{\exp(-A)-1-\exp(-A\delta)+\exp(-A(1-\delta))\}\right.$$

$$\left. + b_3(x)\{1-\delta\}\right] \ ,$$

where $b_1(x)$ is given by (A2.2). The partial derivatives $\partial b_1/\partial\delta$, $\partial b_1/\partial u_f$, $\partial b_1/\partial b_3$, $\partial b_2/\partial\delta$, $\partial b_2/\partial u_f$, $\partial b_2/\partial b_3$ in (A2.8) are the same as defined earlier in (A3.3); and the remaining partial derivatives $\partial I_2/\partial\delta$, $\partial I_2/\partial u_f$, $\partial I_2/\partial b_1$, $\partial I_2/\partial b_2$, $\partial I_2/\partial b_3$ are defined in (A3.4)-(A3.5) of Appendix A3.

Now we note that the coefficient matrix on the left side of (7.13) is such that AA23=0 (see $(7.10)_3$). Using this fact we find its determinant and write it as 'det A'.

$$\det A \equiv AA11(AA22)AA33 - AA12(AA21)AA33 +$$

$$AA13(AA21)AA32 - AA13(AA31)AA22 . \qquad (A2.9)$$

The function on the right side of $(8.1)_4$ are given as

$$f_1(\delta,u_f,b_3) \equiv -\{(AA12)AA33 - (AA32)AA13\}\{1/Re_1Pr_1Ja \det A\}$$

$$-(AA22)(AA13)(g_2/\det A) ,$$

$$f_2(\delta,u_f,b_3) \equiv \{(AA11)AA33 - (AA31)AA13\}\{1/Re_1Pr_1Ja \det A\}$$

$$+(AA21)(AA13)(g_2/\det A) ,$$

$$f_3(\delta,u_f,b_3) \equiv -\{(AA11)AA32 - (AA31)AA12\}\{1/Re_1Pr_1Ja \det A\}$$

$$-\{(AA11)AA22 - (AA21)AA12\}(g_2/\det A) . \qquad (A2.10)$$

Appendix A3

To define the partial derivatives occurring in (A2.6), we use the symbolic manipulation results for the functions b_1, b_2, and I_1 as they occur in their definitions (A2.2), (A2.4), and (A2.5). For the reader to make sense of the definitions, we recommend the following associations for the names of the partial derivatives.

$$\frac{\partial I_1}{\partial \delta} \equiv \text{DI1DD}\,, \quad \frac{\partial I_1}{\partial u_f} \equiv \text{DI1DUF}\,, \quad \frac{\partial I_1}{\partial b_1} \equiv \text{DI1DB1}\,, \quad \frac{\partial I_1}{\partial b_2} \equiv \text{DI1DB2}\,,$$

$$\frac{\partial I_1}{\partial b_3} \equiv \text{DI1DB3}\,, \quad \frac{\partial b_1}{\partial \delta} \equiv \text{DB1DD}\,, \quad \frac{\partial b_1}{\partial u_f} \equiv \text{DB1DUF}\,, \quad \frac{\partial b_1}{\partial b_3} \equiv \text{DB1DB3}\,,$$

$$\frac{\partial b_2}{\partial \delta} \equiv \text{DB2DD}\,, \quad \frac{\partial b_2}{\partial u_f} \equiv \text{DB2DUF}\,, \quad \text{and} \quad \frac{\partial b_2}{\partial b_3} \equiv \text{DB2DB3}\,. \tag{A3.1}$$

Further we make the following association for the variables occurring in the expressions of the above derivatives:

$$\delta \equiv \text{D}\,, \quad u_f \equiv \text{UF}\,, \quad b_1 \equiv \text{B1}\,, \quad b_2 \equiv \text{B2}\,, \quad b_3 \equiv \text{B3}\,, \quad A \equiv \text{A}\,, \quad \frac{\mu_1}{\mu_2} = \text{MU12}\,. \tag{A3.2}$$

We now define the derivatives in (A3.1) using variables in (A3.2) and the usual Maple employment of Fortran symbols for arithmetic operations and exponentiation. The derivatives in (A3.1) are

```
DI1DD = -1/6*1/A*(6*EXP(-A)*A*B1+6*A*B1-6*EXP(-A*D)*A*B1-6*EXP(-A*(1-D))*A*B1+3
*B3*D**2*A-3*B3*A+6*B2*D*A-6*B2*A)

DI1DUF = 0

DI1DB1 = 1/6*1/A*(6*EXP(-A)*A+6*A+6*EXP(-A)-6)-1/6*1/A*(6*EXP(-A)*D*A+6*A*D+6*E
XP(-A*D)-6*EXP(-A*(1-D)))

DI1DB2 = -1/2-1/6*1/A*(3*D**2*A-6*A*D)

DI1DB3 = -1/3-1/6*1/A*(D**3*A-3*A*D)


DB1DD = -1/(A*EXP(-A*D)-A*EXP(-A*(1-D))-(1-EXP(-A*D)-EXP(-A*(1-D))+EXP(-A))/(D-
1))**2*((MU12*(D-1)-D)/D/(D-1)*UF+1/2*B3*(1-D))*(-A**2*EXP(-A*D)-A**2*EXP(-A*(1-
D))-(A*EXP(-A*D)-A*EXP(-A*(1-D)))/(D-1)+(1-EXP(-A*D)-EXP(-A*(1-D))+EXP(-A))/(D-1
)**2)+1/(A*EXP(-A*D)-A*EXP(-A*(1-D))-(1-EXP(-A*D)-EXP(-A*(1-D))+EXP(-A))/(D-1))*
((MU12-1)/D/(D-1)*UF-(MU12*(D-1)-D)/D**2/(D-1)*UF-(MU12*(D-1)-D)/D/(D-1)**2*UF-1
/2*B3)

DB1DUF = 1/(A*EXP(-A*D)-A*EXP(-A*(1-D))-(1-EXP(-A*D)-EXP(-A*(1-D))+EXP(-A))/(D-
1))*(MU12*(D-1)-D)/D/(D-1)

DB1DB3 = 1/(A*EXP(-A*D)-A*EXP(-A*(1-D))-(1-EXP(-A*D)-EXP(-A*(1-D))+EXP(-A))/(D-
1))*(1/2-1/2*D)                                                              (A3.3)

DB2DD = -UF/(D-1)**2+1/(A*EXP(-A*D)-A*EXP(-A*(1-D))-(1-EXP(-A*D)-EXP(-A*(1-D))+
EXP(-A))/(D-1))**2*((MU12*(D-1)-D)/D/(D-1)*UF+1/2*B3*(1-D))*(1-EXP(-A*D)-EXP(-A*
(1-D))+EXP(-A))/(D-1)*(-A**2*EXP(-A*D)-A**2*EXP(-A*(1-D))-(A*EXP(-A*D)-A*EXP(-A*
(1-D)))/(D-1)+(1-EXP(-A*D)-EXP(-A*(1-D))+EXP(-A))/(D-1)**2)-1/(A*EXP(-A*D)-A*EXP
(-A*(1-D))-(1-EXP(-A*D)-EXP(-A*(1-D))+EXP(-A))/(D-1))*((MU12-1)/D/(D-1)*UF-(MU12
*(D-1)-D)/D**2/(D-1)*UF-(MU12*(D-1)-D)/D/(D-1)**2*UF-1/2*B3)*(1-EXP(-A*D)-EXP(-A
*(1-D))+EXP(-A))/(D-1)-1/(A*EXP(-A*D)-A*EXP(-A*(1-D))-(1-EXP(-A*D)-EXP(-A*(1-D))
+EXP(-A))/(D-1))*((MU12*(D-1)-D)/D/(D-1)*UF+1/2*B3*(1-D))*(A*EXP(-A*D)-A*EXP(-A*
(1-D)))/(D-1)+1/(A*EXP(-A*D)-A*EXP(-A*(1-D))-(1-EXP(-A*D)-EXP(-A*(1-D))+EXP(-A))
/(D-1))*((MU12*(D-1)-D)/D/(D-1)*UF+1/2*B3*(1-D))*(1-EXP(-A*D)-EXP(-A*(1-D))+EXP(
-A))/(D-1)**2-1/2*B3

DB2DUF = 1/(D-1)-1/(A*EXP(-A*D)-A*EXP(-A*(1-D))-(1-EXP(-A*D)-EXP(-A*(1-D ))+EXP(
-A))/(D-1))*(MU12*(D-1)-D)/D/(D-1)**2*(1-EXP(-A*D)-EXP(-A*(1-D))+EXP(-A))

DB2DB3 = -1/(A*EXP(-A*D)-A*EXP(-A*(1-D))-(1-EXP(-A*D)-EXP(-A*(1-D))+EXP(-A))/(D
-1))*(1/2-1/2*D)*(1-EXP(-A*D)-EXP(-A*(1-D))+EXP(-A))/(D-1)-1/2*D-1/2
```

To define the partial derivatives of I_2 in (A2.8), we define some new associations (in addition to (A3.1) and (A3.2)) for interpreting the computer expressions for these derivatives. Let

$$\frac{\partial I_2}{\partial \delta} \equiv \text{DI2DD}\,, \quad \frac{\partial I_2}{\partial u_f} \equiv \text{DI2DUF}\,, \quad \frac{\partial I_2}{\partial b_1} \equiv \text{DI2DB1}\,,$$

$$\frac{\partial I_2}{\partial b_2} \equiv \text{DI2DB2}\,, \quad \frac{\partial I_2}{\partial b_3} \equiv \text{DI2DB3}\,. \tag{A3.4}$$

We now define the derivatives of I_2 as

```
DI2DD = B2*B3*D-2*B1*B2*D-B2**2*D**2+2*B2**2*D-EXP(A*D)*B1/EXP(A)*B3-B2*D**3*B3
-2*EXP(A*D)*B1/EXP(A)*B2+B2*B3*D**2-1/4*B3**2*D**4-1/EXP(A*D)*B1*B3-B1/EXP(A)*B3
*D**2+2*1/EXP(A*D)*D*B1*B2-2*B1/EXP(A)*B2*D-B1*B3*D**2-1/EXP(A*D)**2*B1**2+1/EXP
(A*D)*D**2*B1*B3+2*1/EXP(A*D)*B1**2/EXP(A)+2*1/EXP(A*D)*B1**2+1/EXP(A)*EXP(A*D)*
D**2*B1*B3+2*1/EXP(A)*EXP(A*D)*D*B1*B2-EXP(A*D)**2*B1**2/EXP(A)**2+1/2*B3**2*D**
2-2*1/EXP(A*D)*B1*B2+2*EXP(A*D)*B1**2/EXP(A)**2+2*EXP(A*D)*B1**2/EXP(A)-1/4*B3**
2+2*B1/EXP(A)*B2+B1/EXP(A)*B3-B1**2-4*B1**2/EXP(A)+2*B1*B2+B1*B3-B1**2/EXP(A)**2
-B2**2-B2*B3

DI2DUF = 0

DI2DB1 = 2*1/EXP(A)/A**2*B2-4*1/EXP(A*D)/A*B1/EXP(A)-1/EXP(A)*B2*D**2+2*1/EXP(A
)*B2*D-1/3*1/EXP(A)*B3*D**3+2*1/EXP(A*D)/A*B2+4*1/A*EXP(A*D)*B1/EXP(A)**2+2*1/EX
P(A)*EXP(A*D)/A*D*B2-1/A*EXP(A*D)/EXP(A)*B3+1/EXP(A*D)/A*B3-2*1/EXP(A)*EXP(A*D)/
A**2*D*B3-8*B1/EXP(A)*D-2*1/EXP(A*D)/A**3*B3-2*1/EXP(A*D)/A**2*B2+2*1/EXP(A)/A**
2*B3-2*1/EXP(A*D)/A*D*B2-2*1/A*EXP(A*D)/EXP(A)*B2+2*1/EXP(A)*EXP(A*D)/A**3*B3+1/
EXP(A)*EXP(A*D)/A*D**2*B3-EXP(A*D)**2/A*B1/EXP(A)**2-2*1/EXP(A)*EXP(A*D)/A**2*B2
-1/EXP(A*D)/A*D**2*B3-2*1/EXP(A*D)/A**2*D*B3+1/EXP(A)*B3*D-2*B1*D+2*1/A**2*B2+4*
1/A*EXP(A*D)*B1/EXP(A)+2*B1/EXP(A)**2-3*1/A*B1-4*1/EXP(A*D)/A*B1+1/EXP(A*D)**2/A
*B1+3*1/EXP(A)**2/A*B1-B2*D**2+2*B2*D+B3*D-2*1/A**3*B3-2/3*1/EXP(A)*B3-1/EXP(A)*
B2-1/3*B3*D**3-2*B1/EXP(A)**2*D+2*1/EXP(A)/A**3*B3+8*B1/EXP(A)+2*1/A**2*B3+2*B1-
B2-2/3*B3

DI2DB2 = 2*1/A**2*B1+2*1/EXP(A)/A**2*B1-1/4*D**4*B3-2*1/EXP(A*D)/A**2*B1-B3*D+2
*B1*D-B1*D**2-2/3*B2*D**3-2*1/EXP(A*D)/A*D*B1+2*B2*D**2-2*B2*D+1/3*B3*D**3-2*1/A
*EXP(A*D)*B1/EXP(A)+1/2*B3*D**2-2*1/EXP(A)*EXP(A*D)/A**2*B1+2*1/EXP(A)*EXP(A*D)/
A*D*B1-B1/EXP(A)*D**2+2*B1/EXP(A)*D+2*1/EXP(A*D)/A*B1-B1/EXP(A)-B1+2/3*B2+5/12*B
3

DI2DB3 = -1/3*B1/EXP(A)*D**3-1/10*B3*D**5+B1/EXP(A)*D-1/EXP(A*D)/A*D**2*B1+B1*D
-2*1/EXP(A*D)/A**2*D*B1-1/A*EXP(A*D)*B1/EXP(A)-1/4*B2*D**4-1/3*B1*D**3-2*1/EXP(A
)*EXP(A*D)/A**2*D*B1+1/EXP(A*D)/A*B1+1/EXP(A)*EXP(A*D)/A*D**2*B1+2*1/EXP(A)*EXP(
A*D)/A**3*B1-2*1/A**3*B1+1/2*B2*D**2-B2*D-1/2*B3*D+2*1/A**2*B1+1/3*B3*D**3+1/3*B
2*D**3-2*1/EXP(A*D)/A**3*B1+2*1/EXP(A)/A**2*B1+2*1/EXP(A)/A**3*B1-2/3*B1/EXP(A)-
2/3*B1+5/12*B2+4/15*B3
```

(A3.5)

References

1. Jacobs, H.R., 1988. Direct Contact Condensation in *Direct Contact Heat Transfer*, 1988. Edited by Krieth, F. and Boehm, R.F, Hemisphere Publishing.

2. Vallano, R.W. and DeBellis, D.E., May 1984. State of Technology of Direct Contact Heat Exchanging, U.S.D.O.E. Report No. PNL-5008, Pacific Northwest Laboratories, Battelle Memorial Institute, Richland, WA.

3. Fisher, E.M. and Wright, J.D., May 1984. Direct Contact Condensers for Solar Pond Production. U.S.D.O.E. Report SERI/TR-252-2164, Solar Energy Research Institute, Golden, CO.

4. Nusselt, W., 1916. Die Oberflächenkondesation des Wasserdampfes, *Z. Ver. Dt. Ing.* **60** (27), 541-546.

5. Rohsenow, W.M., 1956. Heat Transfer and Temperature Distribution in Laminar Film Condensation, *Transactions ASME* **78**, 1645-1648.

6. Sparrow, E.M. and Gregg, J.L., 1959. A boundary layer treatment of laminar film condensation, *J. Heat Transfer (ASME)* **81**, 13-18.

7. Ford, J.D. and Lekic, A., 1973. Rate of Growth of Drops During Condensation. *Internat. Journal of Heat and Mass Transfer* **16**, 61-66.

8. Jacobs, H.R. and Cook, D.S., August 1978. Direct Contact Condensation on a Non-Circulating Drop. Proceedings of the 6th Internat. Heat Transfer Conf., *Heat Transfer 1978* **3**, 389-393, Toronto, Canada.

9. Sundararajan, T. and Ayyaswamy, P.S., 1974. Hydrodynamics and Heat Transfer associated with condensation on a moving drop: Solutions for Intermediate Reynolds Numbers. *J. Fluid Mech.* **149**, 33-58.

10. Soliman, M., Schuster, J.R., and Berenson, P.J., 1968. A general heat transfer correlation for annular flow condensation. *J. Heat Transfer* (**90**) 267-276.

11. Chaddock, J.B., 1957. Film Condensation of vapor in a horizontal tube. *Refrigerating Engineering* **65**, 36-41.

12. Chato, J.C., 1962. Laminar condensation inside horizontal tube. *ASHRAE Journal* **4**, 52-60.

13. Rufer, C.E. and Kezios, S.P., 1966. Analysis of two-phase, one-component, stratified flow with condensation. *J. Heat Transfer*, **88**(2), 265-275.

14. Lucas, K. and Moser, B., 1979. Laminar film condensation of pure vapors in tubes. *Int. J. of Heat and Mass Transfer* **22**, 431-435.

15. Narain, A., and Kan Lee, 1989 (to appear). Interfacial Stability and Stability mechanisms for the flow of pure vapor undergoing film condensation over a cold horizontal plate.

16. Delhaye, J.M., 1974. Jump Conditions and Entropy Sources in Two-Phase Systems: Local Instant Formulation. *Int. J. of Multiphase Flow* **1**, 395-409.

17. Delhaye, J.M., 1976. Local Instantaneous Equations in *Two-Phase Flows and Heat Transfer*, Vol. 1, Proceedings of NATO Advanced Study Institute, Aug. 16-27, 1976. Istanbul, Turkey. Edited by S. Kakac and F. Mayinger.

18. Whitaker, S., 1977. *Fundamental Principles of Heat Transfer*, Pergamon Press.

19. Arpaci, V.S. and Larsen, P.S., 1984. *Convection Heat Transfer*, Prentice Hall.

20. Sparrow, E.M., Patankar, S.V., and Ramadhyani, S., 1977. Analysis of melting in the presence of natural convection in the melt region, *J. Heat Transfer* **99**, 520.

21. Theodore von Kármán, 1921. Über Laminare und turbulente Reibung, *ZAMM* **1**, 233-252. See also NACA Tech. Memo. 1092 (1946).

22. Pohlhausen, K., 1921. Zur näherungsweisen Integration der Differentialgleichung der laminaren Reibungsschicht, *ZAMM* **1**, 252-268.

23. Christodoulou, C., 1988. Condensation in a Horizontal Rectangular Duct. An Experimental Study. M.S. Thesis, (adviser: N.V. Suryanarayana) Michigan Technological University, Houghton, MI 49931 (USA).

24. Koh, J.C.Y., 1962. Film condensation in a forced-convection boundary-layer flow. *Int. J. Heat Mass Transfer* **5**, 941-954.

25. Koh, J.C.Y., Sparrow, E.M., and Hartnett, J.P., 1961. The two phase boundary layer in laminar film condensation. *Int. J. Heat Mass Transfer* **2**, 69-82.

26. ASHRAE Handbook, 1985 Fundamentals SI Edition, American Society of Heating, Refrigerating and Air-Conditioning Engineers, Inc., Atlanta, GA.

27. Batchelor, G.K., 1981. *An Introduction to Fluid Dynamics*, Cambridge University Press.

28. Van Wylen, G.J. and Sonntag, R.E., 1985. *Fundamentals of Classical Thermodynamics*, Wiley.

29. White, F.M., 1974. *Viscous Fluid Flow*, McGraw Hill.

30. Ruckenstien, E. and Jain, R.K., 1974. Spontaneous Rupture of Thin Liquid Films. *Chem. Soc. Faraday Trans.* **II** (70), 132-147.

31. Weatherburn, C.E., 1927. Differential Geometry of Three Dimensions, Cambridge University Press.

32. Kocamustafaogullari, G., 1985. Two-Fluid Modelling in Analyzing the Interfacial Stability of Liquid Film Flows, *Int. J. Multiphase Flow,* **11** (1), 63-89.

33. Truesdell, C.A. and Toupin, R.A., 1960. *The Classical Field Theories*, Flügge's Handbuch der Physik, III/1, Berlin-Götingen-Heidelberg: Springer.

34. Schlichting, H., 1979. *Boundary Layer Theory*, Seventh Edition, McGraw Hill.

35. Kizilyalli, Y., 1989. Computations for flow of pure vapor undergoing film condensation between two parallel plates. M.S. Thesis (Mechanical Engineering), Michigan Technological University, Houghton, MI.